J. Fluid Mech. (1973), *vol.* 60, *part* 2, *pp.* 321–362
Printed in Great Britain

The laser-Doppler velocimeter and its application to the measurement of turbulence

By WILLIAM K. GEORGE
Applied Research Laboratory, The Pennsylvania State University
AND JOHN L. LUMLEY
Department of Aerospace Engineering, The Pennsylvania State University

(Received 31 January 1973)

In 1964, Yeh & Cummins demonstrated that coherent light sources could be used for the measurement of steady fluid velocities by observing the Doppler shift in the frequency of light scattered from small particles moving with the fluid. Since 1964 many investigators have attempted to extend this technique to the measurement of turbulent velocity fluctuations.

A fundamental limitation on this type of velocimeter is the Doppler ambiguity introduced by the finite transit time of particles through the scattering volume, turbulent velocity fluctuations across the scattering volume, mean velocity gradients and electronic noise. A unified account of the effect of the Doppler ambiguity on the measurement of the instantaneous velocities is presented and results are interpreted using the power spectrum. The influence of the ambiguity on the measurement of other statistical quantities is also examined.

Limitations on the spatial and temporal resolution imposed by the finite sampling volume are examined using the power spectrum and criteria for optimization of the response are proposed.

An operational laser-Doppler velocimeter is described and measurements of spectra in both laminar and turbulent flow are presented. The experimental results are seen to be in excellent agreement with theoretical predictions.

Part 1. Theoretical investigation

1. Introduction

1.1. *Historical background*

In 1964, Yeh & Cummins successfully measured velocity profiles in a liquid by examining the frequency shift in monochromatic radiation scattered from particles in the liquid. The scattered and unscattered radiation was heterodyned on a photocell producing an electrical signal at the difference frequency; the spectrum of this difference frequency was examined by conventional techniques. Since 1964, numerous investigators have applied this technique to the measurement of mean-square fluctuating velocities and instantaneous velocities in the unsteady flow of gases and liquids (Foreman, Lewis & Thornton 1966; Pike *et al.* 1967; Welch & Tomme 1967; Lumley, George & Kobashi 1969). Recent attempts have been made to measure turbulence in the atmosphere and ocean using radar and sonar as incident radiation (Wiseman 1969; Little 1969; Lhermitte 1968).

1.2. *Nature of the problem*

Considerable attention has been given in the literature to the choice of optical components, scattering particles and electronic signal processing (Huffaker, Fuller & Lawrence 1969; Mayo 1969; Davis 1968; Rolfe *et al.* 1968). The sources of noise have been identified and theory for optimization of the signal-to-noise ratio has been developed. In spite of these advances, the most basic question has not been answered; that is, how does the instantaneous Doppler frequency relate to the instantaneous flow velocity?

The fundamental problem in attempting to relate the Doppler frequency and the flow velocity is that even in a steady laminar flow the Doppler frequency is not steady. The signal received by the photocell is the sum of the signals produced by all the scatterers present in the scattering volume at that instant; the individual signals may have the same frequency, but each has a phase dependent on its position in the scattering volume at some arbitrarily chosen origin in time as well as an intensity dependent on position and particle size.

Additional problems in interpretation arise from the fact that in unsteady or non-uniform flow particles at different locations in the sampling volume may be moving at different velocities. The velocimeter sees a spatial average of these velocities; the result is a loss in spatial resolution and the introduction of additional random phase fluctuations.

1.3. *The scope of this investigation*

Part 1 of this paper will first examine the spatial and temporal resolution of the laser-Doppler velocimeter and criteria for meaningful measurements will be established. Second, the effect of the random phase fluctuations introduced by the Doppler ambiguity on attempts to measure statistical quantities in turbulent flow will be examined. In part 2 an operational laser-Doppler velocimeter will be described and measurements in both laminar and turbulent flow will be presented.

2. A description of the velocimeter

2.1. *The photoelectric current*

The typical laser-Doppler velocimeter employs a scattering beam which is focused at some region in the flow, part of whose light is scattered from neutrally buoyant particles suspended in the flow. This scattered radiation is collected by a photocell and mixed with a reference beam.

The current produced by the photocell is given by the integral over the photosensitive surface of the intensity of the light striking it; hence

$$i_{\text{tot}} = M \iint_S |E_r(x'', y_d'', z) + \sum_k E_{s_k}(x'', y_d'', z)|^2 \, dx'' \, dz, \tag{2.1.1}$$

where M is the photoelectric constant of the photocell, S is the photosensitive area, E_r is the complex amplitude of the reference beam at the photocell and E_{s_k} is the complex amplitude of the light scattered from the kth particle, where

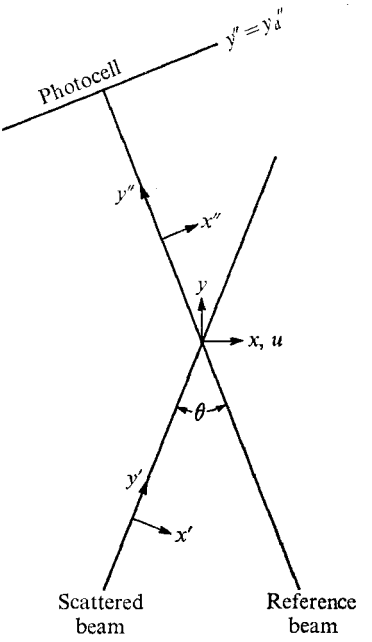

FIGURE 1. Scattering co-ordinates. Origin of all co-ordinate systems is chosen at centre of scattering volume (z is normal to plane of paper).

the co-ordinates are defined by figure 1, and where the summation is over all the scattering particles. Expanding (2.1.1), we have

$$i_{\text{tot}} = M \iint_S \{E_r E_r^* + E_r \sum_k E_{s_k}^* + E_r^* \sum_k E_{s_k} + \sum_{kl} E_{s_k} E_{s_l}^*\} dx'' dz, \quad (2.1.2)$$

where * denotes the complex conjugate.

The first term of the integral may be identified as the self-beating of the reference beam. The spectrum of these laser amplitude fluctuations is centred at zero frequency and at frequencies corresponding to the mode spacing of the laser. If these bands do not overlap the Doppler shift spectrum, this term may be removed by filtering (cf. Edwards *et al.* 1971).

The last term contributes to the total current in three frequency bands: in the frequency range from zero to a value representative of the maximum velocity *differences* in the volume, in a similar symmetric interval around twice the mean Doppler frequency, and finally in a band around the mean Doppler frequency owing to the heterodyning of the forward-scattered reference beam (assuming this passes through the flow) and the Doppler-shifted light from the scattering beam. Because of phase cancellation resulting from the fact that the scattering volume is many light wavelengths across, only the $i = j$ (diagonal) terms of the double summation will contribute to the current. If the scattering particles are modelled as spherical radiators, the primary effect of this term may be shown to be to restore the scattered part of the reference beam; hence, the double summation term may be ignored.

For convenience, we shall define

$$i = M \iint_S E_r^* \sum_k E_{s_k} \, dx'' \, dz \tag{2.1.3}$$

as the complex current. Changing the order of summation and integration in (2.1.3) we have

$$i = M \sum_k \iint_S E_r^* E_{s_k} \, dx'' \, dz. \tag{2.1.4}$$

Thus the net current i is simply the sum of the currents generated by each individual scattering particle; we may write the current for a typical particle as i_{sp}, where

$$i_{sp} = M \iint_S E_r^*(x'', y_d'', z) \, E_{sp}(x'', y_d'', z) \, dx'' \, dz. \tag{2.1.5}$$

If the scattering particles are small compared with the wavelength λ, of the light, they may be modelled as spherical radiators (van de Hulst 1957). We write

$$E_{sp}(\mathbf{R}) = \frac{C_p}{j\lambda |\mathbf{R} - \mathbf{x}_p''|} E_i(\mathbf{x}_p') \exp\{jk|\mathbf{R} - \mathbf{x}_p''|\}, \tag{2.1.6}$$

where $j \equiv \sqrt{-1}$ and we have taken

$$\mathbf{R} = (x'', y_d'', z)$$

and

$$|\mathbf{R} - \mathbf{x}_p''|^2 = (x'' - x_p'')^2 + (y_d'' - y_p'')^2 + (z'' - z_p'')^2,$$

where $\mathbf{x}_p$ denotes the scattering-particle co-ordinates and C_p is the scattering coefficient chosen in the manner of Mayo (1970). Substituting (2.1.6) into (2.1.5) we have

$$i_{sp} = MC_p E_i(\mathbf{x}_p') \left\{ \iint_S E_r^*(\mathbf{R}) \frac{\exp\{jk|\mathbf{R} - \mathbf{x}_p''|\}}{j\lambda |\mathbf{R} - \mathbf{x}_p''|} \, dx'' \, dz \right\}. \tag{2.1.7}$$

The term in curly brackets has been identified by Mayo (1970) as the inverse propagation convolution of $E_r(x'', y_d'', z)$ and therefore specifies the form of the reference beam at the position of the particle, that is $E_r(x_p'', y_p'', z_p)$. Thus

$$i_{sp} = MC_p E_i(x_p', y_p', z_p) \, E_r^*(x_p'', y_p'', z_p), \tag{2.1.8}$$

where it should be noted that E_i and E_r are expressed in different co-ordinate systems. Mayo (1970) has shown that, by defining an equivalent reference beam, an equation for i_{sp} of the form of (2.1.8) may be obtained even when there are spatial filters between the scattering volume and the photocell. It should be noted that those results were obtained by ignoring the obliquity factor of scalar diffraction theory (cf. Goodman 1968) and the difference between the wavelengths of the incident and scattered light. The first assumption is valid for small aperture and the second for particle velocities well below that of light (cf. Lading 1970).

Usually $E_i(x', y', z)$ and $E_r(x'', y'', z)$ are determined by focusing Gaussian cross-section beams to their diffraction-limited spot sizes at the desired flow locations; hence,

$$\left.\begin{aligned} E_r(x'', y'', z) &= E_{0r} \exp\{-(x''^2 + z^2)/2\sigma^2\} \exp\{j(2\pi y''/\lambda)\}, \\ E_i(x', y', z) &= E_{0i} \exp\{-(x'^2 + z^2)/2\sigma^2\} \exp\{j(2\pi y'/\lambda)\}, \end{aligned}\right\} \tag{2.1.9}$$

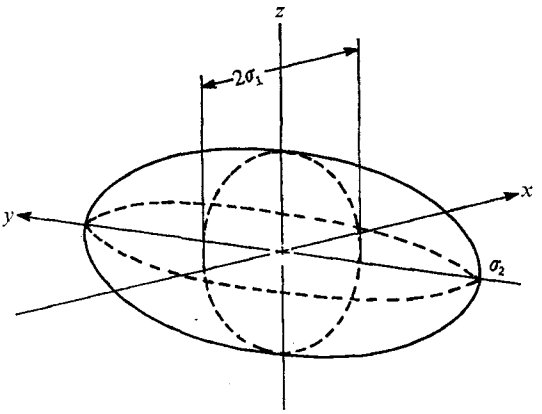

FIGURE 2. Scattering volume for $\theta = 45°$.

where E_{0r} and E_{0i} are the amplitudes at the centre of focus and where σ is given by

$$\sigma = \frac{2^{\frac{1}{2}} f_0 \lambda}{\pi d}, \tag{2.1.10}$$

f_0 is the focal length of the lens and d is the distance between the $1/e^2$ intensity points of the beam at the lens. For convenience we have chosen the focal lengths of the two lenses to be equal to facilitate interpretation of results. Also, the depth of focus has been ignored since for all reasonable values of the parameters it is larger than the effective beam cross-section defined by (2.1.11); hence, the beam cross-sections are considered constant along the direction of propagation near the focal point.

Substitution of (2.1.9) into (2.1.8) and transformation to the velocimeter co-ordinate system $\mathbf{x}$ (see figure 1) yields

$$i_{sp} = \tfrac{1}{2} I \exp\{-[x_p^2 \cos^2 \tfrac{1}{2}\theta + y_p^2 \sin^2 \tfrac{1}{2}\theta + z_p^2]/\sigma^2\} \exp\{j4\pi\lambda^{-1} x_p \sin \tfrac{1}{2}\theta\}, \tag{2.1.11}$$

where $\mathbf{x}_p = (x_p, y_p, z_p)$ represents the co-ordinates of the scattering particle in the velocimeter co-ordinate system and where we have defined

$$I = 2MC_p E_{0r} E_{0i}. \tag{2.1.12}$$

(Note that we have not restricted the direction of the mean flow to correspond to the x direction.) Clearly

$$\sigma_1 = \sigma/2^{\frac{1}{2}} \cos \tfrac{1}{2}\theta, \quad \sigma_2 = \sigma/2^{\frac{1}{2}} \sin \tfrac{1}{2}\theta, \quad \sigma_3 = \sigma/2^{\frac{1}{2}} \tag{2.1.13}$$

represent characteristic dimensions of the scattering volume (see figure 2) and

$$K = (4\pi/\lambda) \sin \tfrac{1}{2}\theta \tag{2.1.14}$$

represents a scattering wavenumber for the velocimeter configuration.

We may now write the real current from a single scattering particle as

$$i_s = I \exp -\left\{\frac{x^2}{2\sigma_1^2} + \frac{y^2}{2\sigma_2^2} + \frac{z^2}{2\sigma_3^2}\right\} \cos Kx, \tag{2.1.15}$$

where we have dropped the subscript p. Note that I is the amplitude of the current produced by the particle when at the centre of the scattering volume.

2.2. *The signal from moving particles*

If we define $\mathbf{a} = (a, b, c)$ to be the initial position of the scattering particle which at time t is at $\mathbf{x} = (x, y, z)$, we may write

$$\left.\begin{aligned} x(\mathbf{a},t) &= a + \int_0^t U(\mathbf{a},t_1)\,dt_1, \\ y(\mathbf{a},t) &= b + \int_0^t V(\mathbf{a},t_1)\,dt_1, \\ z(\mathbf{a},t) &= c + \int_0^t W(\mathbf{a},t_1)\,dt_1, \end{aligned}\right\} \tag{2.2.1}$$

where $\mathbf{U}(\mathbf{a},t) = [U(\mathbf{a},t), V(\mathbf{a},t), W(\mathbf{a},t)]$ is the particle velocity.

It is clear from (2.1.15) that the instantaneous phase of the signal from a single scatterer is given by Kx. Using (2.2.1) we may separate this phase into a fixed phase γ and a time-dependent phase $\Omega(t)$, where

$$\gamma = Ka \tag{2.2.2}$$

and

$$\Omega(t) = K\int_0^t U(\mathbf{a},t_1)\,dt_1. \tag{2.2.3}$$

The rate of change of phase $d\Omega/dt$ is easily seen to be proportional to the particle velocity, i.e.

$$\frac{d\Omega}{dt} = K\frac{d}{dt}\int_0^t U(\mathbf{a},t_1)\,dt_1 = KU(\mathbf{a},t). \tag{2.2.4}$$

If the scattering particle is assumed to move with the local fluid velocity, then $U(\mathbf{a},t)$ is the Lagrangian fluid velocity or the *material* velocity (cf. Serrin 1959), which depends only on the initial position $\mathbf{a}$ of the fluid particle and the time t.

It is clear from (2.1.5), (2.2.1) and (2.2.4) that if *no more than one* particle at a time is in the scattering volume, one need only count the zero crossings of the signal to obtain the velocity. If this procedure is repeated many times, the probability density of particle velocities may be obtained; the measurements are contaminated only by the resolution of the counting techniques used. All real time information is, of course, lost since the particles arrive randomly.

In the remainder of this paper *we shall restrict ourselves to situations where the expected number of scattering particles in the scattering volume is greater than one.* Since, with this restriction, the velocimeter output consists of contributions from many particles, identification of the rate of change of phase of the Doppler current with the Eulerian velocity at the scattering volume will not be without ambiguities.

We shall define an effective velocity 'seen' by the velocimeter as the instantaneous velocity averaged over all scattering particles contributing to the Doppler signal, i.e.

$$u_0(t) = \frac{1}{\mu}\iiint_{\text{all space}} U(\mathbf{a},t)\,g(\mathbf{a})\,w[x(\mathbf{a},t)]\,d\mathbf{a}, \tag{2.2.5}$$

where $g(\mathbf{a})$ is a random weighting function which accounts for the presence or absence of the scattering particles as well as their size, where $w(\mathbf{x})$ is a deterministic function with random argument which accounts for spatial variations in the Doppler current and, in effect, defines the scattering volume, and where μ is the expected number of scattering particles per unit volume. For the situation described above $w(\mathbf{x})$ is given by

$$w(\mathbf{x}) = \frac{1}{(2\pi)^{\frac{3}{2}}\sigma_1\sigma_2\sigma_3} \exp - \left\{ \frac{x^2}{2\sigma_1^2} + \frac{y^2}{2\sigma_2^2} + \frac{z^2}{2\sigma_3^2} \right\}. \tag{2.2.6}$$

For a monodisperse collection of point-scattering particles, $g(\mathbf{a})$ is the familiar Dirac delta function $\delta(\mathbf{a})$ at each particle location. The statistics of g are developed in the appendix. For a finite scattering volume with $w(\mathbf{x})$ = constant over the region of definition and zero elsewhere, (2.2.5) is mathematically equivalent to

$$u_0(t) = \frac{1}{N_i} \sum_{n=1}^{N_i} U(\mathbf{a}_n, t), \tag{2.2.7}$$

where N_i is the instantaneous number of scattering particles in the scattering volume. We shall see later that the V and W velocity components may be accounted for separately and that $u_0(t)$ corresponds to the Eulerian velocity, which we intuitively feel should be measured by a spatially fixed instrument.

We now may define, using (2.2.5), an effective displacement $X(t)$ by

$$X(t) = \int_0^t u_0(t_1)\, dt_1. \tag{2.2.8}$$

Using (2.2.1) and (2.2.8) we may write the x co-ordinate of a particle as

$$x(t) = a + X(t) + \Delta(\mathbf{a}, t), \tag{2.2.9}$$

where

$$\Delta(\mathbf{a}, t) = \int_0^t [U(\mathbf{a}, t_1) - u_0(t_1)]\, dt_1. \tag{2.2.10}$$

Clearly, $\Delta(\mathbf{a}, t)$ is a Lagrangian property and represents the deviation of the particle displacement from the average displacement over the field.

By combining (2.2.9) and (2.1.15) we may obtain an expression for the current produced by a single particle with the Eulerian information occurring explicitly.

2.3. *The total Doppler signal*

From (2.1.4), (2.1.15) and (2.2.9) we may write the total Doppler current as

$$i(t) = \sum_m I \exp - \left\{ \frac{x_m^2}{2\sigma_1^2} + \frac{y_m^2}{2\sigma_2^2} + \frac{z_m^2}{2\sigma_3^2} \right\} \cos K[a_m + X + \Delta_m], \tag{2.3.1}$$

where (x_m, y_m, z_m) and (a_m, b_m, c_m) represent respectively the position and initial position of the mth particle and where, as before, the summation is over all scattering particles.

Since the scattering volume is actually unbounded, the number of scattering

particles is infinite and (2.3.1) is inconvenient. We may write the total Doppler current in a more convenient form as

$$i(t) = \int_{\text{all space}} i(t,\mathbf{a})\, g(\mathbf{a})\, d\mathbf{a}, \tag{2.3.2}$$

where $i(t,\mathbf{a})$ is the current generated by a single particle and where, as before, $g(\mathbf{a})$ is its strength at each initial position. We note that both $i(t,\mathbf{a})$ and $g(\mathbf{a})$ are random functions: $i(t,\mathbf{a})$ because of its dependence on the random displacement field of the turbulence and $g(\mathbf{a})$ because of its dependence on the (random) presence or absence of a particle. The representation (2.3.2) is an extension of that used by Rice (1954) for shot noise (cf. Lumley 1970, p. 80).

Since the particles are randomly located in the flow, $g(\mathbf{a})$ is statistically independent for different values of $\mathbf{a}$. Hence, $i(t)$ is the sum of a large number of statistically independent random variables whose absolute third moments may be chosen to be bounded; we have by the central limit theorem (cf. Lumley 1970, p. 30) that the characteristic functional of $i(t)$ is Gaussian in the limit of many particles. In fact, it can be shown that the approach of the characteristic functional to Gaussian is inversely proportional to the square root of the effective number of scattering particles defined by $\mu\sigma_1\sigma_2\sigma_3$, where μ is the expected number of particles per unit volume.

By defining

$$F(t) = \int_{\text{all space}} \exp-\left\{\frac{x^2}{2\sigma_1^2}+\frac{y^2}{2\sigma_2^2}+\frac{z^2}{2\sigma_3^2}\right\} \cos K[a+\Delta(\mathbf{a},t)]\, g(\mathbf{a})\, d\mathbf{a} \tag{2.3.3}$$

and

$$G(t) = -\int_{\text{all space}} \exp-\left\{\frac{x^2}{2\sigma_1^2}+\frac{y^2}{2\sigma_2^2}+\frac{z^2}{2\sigma_3^2}\right\} \sin K[a+\Delta(\mathbf{a},t)]\, g(\mathbf{a})\, d\mathbf{a} \tag{2.3.4}$$

we can write (2.3.2.) as

$$i(t) = F(t)\cos KX + G(t)\sin KX. \tag{2.3.5}$$

From the definitions and by reasoning of the same kind as was applied to $i(t)$, it is straightforward to show that F and G are also Gaussian random variables.

Using a well-known trigonometric identity, we have

$$i(t) = (F^2+G^2)^{\frac{1}{2}} \cos(KX-\phi), \tag{2.3.6}$$

where

$$\phi = \tan^{-1}(G/F). \tag{2.3.7}$$

A typical detector removes the amplitude information by amplifying and clipping and keeps only information on the zero crossings, giving a signal proportional to frequency, say ω_1, where

$$\omega_1 = K\frac{dX}{dt} - \frac{d\phi}{dt}, \tag{2.3.8}$$

or

$$\omega_1 = Ku_0(t) - \dot{\phi}. \tag{2.3.9}$$

We have thus obtained not only the Eulerian-like velocity which we sought, but also a term representing the random phase fluctuations introduced by the particle motion. It remains to be shown that $u_0(t)$ and $\dot{\phi}$ are statistically independent or at least uncorrelated. Before proceeding to an examination of the statistics of ω_1, we shall first analyse $u_0(t)$ – particularly its dependence on the u component of the Eulerian velocity field $u(x,y,z,t)$.

3. Spatial and temporal resolution

3.1. *The spectrum of* $u_0(t)$

The mean-square fluctuation of $u_0(t)$ is given by

$$\overline{u_0'(t)^2} = \overline{[u_0(t) - \overline{u_0(t)}]^2}, \tag{3.1.1}$$

where $\overline{u_0(t)}$ is the expected value of $u_0(t)$. From (2.2.5) it follows that

$$\overline{u_0(t)} = \frac{1}{\mu}\int_{\text{all space}} \overline{U(\mathbf{a},t)\, g(\mathbf{a})\, w[\mathbf{x}(\mathbf{a},t)]}\, d\mathbf{a} \tag{3.1.2a}$$

$$= \frac{1}{\mu}\int_{\text{all space}} \overline{U(\mathbf{x},t)\, g(\mathbf{x})\, w(\mathbf{x})}\, d\mathbf{x} = \int_{\text{all space}} \overline{u(\mathbf{x},t)}\, w(\mathbf{x})\, d\mathbf{x} \tag{3.1.2b,c}$$

if the fluid is assumed incompressible (cf. Lumley 1961). It is clear from (3.1.2*c*), that, if the mean velocity profile has appreciable curvature across the scattering volume, u_0 will not correspond to the velocity at the centre of the volume. This has been previously pointed out by Edwards *et al.* (1971) for laminar flows and is certainly of primary importance in many capillary flows.

If the mean velocity profile is constant (or linear) across the scattering volume, we have

$$\overline{u_0(t)} = \overline{u(\mathbf{x},t)} \int w(\mathbf{x})\, d\mathbf{x}$$

$$= \overline{u(\mathbf{x},t)}. \tag{3.1.3}$$

Thus the mean value of $u_0(t)$ is identical to the average Eulerian velocity at the centre of the scattering volume under the above restrictions.

We compute the mean-square effective velocity in a similar fashion:

$$\overline{u_0'^2} = \overline{(u_0 - \bar{u}_0)^2}$$

$$= \overline{\left\{\frac{1}{\mu}\int [u(\mathbf{x},t)\, g(\mathbf{x}) - \overline{u(\mathbf{x})}\,\overline{g(\mathbf{x})}]\, w(\mathbf{x})\, dx\right\}^2}$$

$$= \frac{1}{\mu^2}\iint \overline{u(\mathbf{x},t)\, u(\mathbf{x}',t)}\,\overline{g(\mathbf{x})\, g(\mathbf{x}')}\, w(x)\, w(\mathbf{x}')\, d\mathbf{x}\, d\mathbf{x}' - \frac{1}{\mu^2}\left\{\int \overline{u(\mathbf{x},t)}\,\overline{g(\mathbf{x})}\, w(\mathbf{x})\, d\mathbf{x}\right\}^2. \tag{3.1.4}$$

Using (see appendix)

$$\overline{g(\mathbf{x})\, g(\mathbf{x}')} = \mu^2 + \mu\delta(\mathbf{x}-\mathbf{x}') \tag{3.1.5}$$

and

$$R_{11}(x,x') = \overline{[u(\mathbf{x},t) - \overline{u(\mathbf{x})}]\,[u(\mathbf{x}',t) - \overline{u(\mathbf{x}')}]} \tag{3.1.6}$$

we have

$$\overline{u_0'^2} = \int R_{11}(\mathbf{x},\mathbf{x}')\, w(\mathbf{x})\, w(\mathbf{x}')\, d\mathbf{x}\, d\mathbf{x}' + \frac{1}{\mu}\int \overline{u^2}(\mathbf{x})\, w^2(\mathbf{x})\, d\mathbf{x}. \tag{3.1.7}$$

For homogeneous turbulence $\overline{u^2}$ is independent of $\mathbf{x}$ and

$$\frac{1}{\mu}\int w^2(x)\, dx \equiv \frac{1}{\mu V}, \tag{3.1.8}$$

where V can be taken as the effective volume. But μV is the average number of scattering particles in the effective volume, say N_V, and we can write

$$\overline{u_0'^2} = \int \Phi_{11}(\mathbf{k})\, \mathscr{W}(\mathbf{k})\, dk + \frac{1}{N_V}(\overline{u'^2} + \overline{u}^2), \tag{3.1.9}$$

where $\Phi_{11}(\mathbf{k})$ is the u-velocity spectrum and $\mathscr{W}(\mathbf{k})$ is defined by

$$\mathscr{W}(k) = \hat{w}(k)\, \hat{w}^*(k), \tag{3.1.10}$$

where $\hat{w}(k)$ is the Fourier transform of $w(\mathbf{x})$. We may rewrite this as

$$\overline{u_0'^2} = \int \Phi_{11}(\mathbf{k}) \left\{ \mathscr{W}(\mathbf{k}) + \frac{1}{N_V} \right\} d\mathbf{k} + \frac{1}{N_V}\overline{u}^2. \tag{3.1.11}$$

In the usual case, to which we restrict ourselves, $N_V \gg 1$ and the half-power points of $\mathscr{W}(\mathbf{k})$ are at high wavenumbers relative to the turbulence; thus we shall neglect all but the first term. The neglected terms can be shown to arise from averaging through periods in which there is no signal. (It should be noted that the last term will result in a contribution at zero frequency in the spectrum and, equivalently, a time-independent non-zero correlation. This will be of importance when $(u'^2 N_V/\overline{u}^2) \sim O(1)$.)

From the definition of $w(\mathbf{x})$ given in (2.2.6)

$$\mathscr{W}(\mathbf{k}) = \exp - \left\{ \frac{k_1^2}{2k_*^2} + \frac{k_2^2}{2m_*^2} + \frac{k_3^2}{2n_*^2} \right\}, \tag{3.1.12}$$

where $\mathbf{k} = (k_1, k_2, k_3)$ are the wavenumber components of spatial variations in the (x, y, z) directions respectively and where (k_*, m_*, n_*) are wavenumbers defined from the scattering volume parameters as

$$k_* = 1/2^{\frac{1}{2}}\sigma_1, \quad m_* = 1/2^{\frac{1}{2}}\sigma_2, \quad n_* = 1/2^{\frac{1}{2}}\sigma_3. \tag{3.1.13}$$

It is clear from (3.1.4)–(3.1.7) and (3.1.13) that spatial variations in velocity smaller than the extent of the scattering volume will be attenuated.

The one-dimensional velocity spectrum of the turbulence is defined by

$$F_{11}^1(k_1) = \iint_{-\infty}^{\infty} \Phi_{11}(k_1, k_2, k_3)\, dk_2\, dk_3, \tag{3.1.14}$$

where

$$\overline{u'^2} = \int_{-\infty}^{\infty} F_{11}^1(k_1)\, dk_1. \tag{3.1.15}$$

Using (3.1.11) we define

$$F_0(k_1) = \exp\left\{ -\frac{k_1^2}{2k_*^2} \right\} \iint_{-\infty}^{\infty} \Phi_{11}(k_1, k_2, k_3) \exp\left\{ -\frac{k_2^2}{2m_*^2} - \frac{k_3^2}{2n_*^2} \right\} dk_2\, dk_3, \tag{3.1.16}$$

where

$$\overline{u_0'(t)^2} = \int_{-\infty}^{\infty} F_0(k_1)\, dk_1. \tag{3.1.17}$$

The relation between $F_0(k_1)$, the measured spectrum, and the true spectrum is, of course, of great interest.

If we restrict ourselves to isotropic turbulence we may write (cf. Batchelor 1960, p. 49)

$$\Phi_{11}(k_1, k_2, k_3) = (E(k)/4\pi k^4)\,[k^2 - k_1^2], \tag{3.1.18}$$

where $k^2 = k_1^2 + k_2^2 + k_3^2$ and $E(k)$ is the three-dimensional spectrum function (cf. Batchelor 1960). Using (3.1.18) one may show that

$$F_{11}^1(k_1) = \frac{1}{2}\int_{k_1}^{\infty} \frac{E(k)}{k}\left[1 - \left(\frac{k_1^2}{k^2}\right)\right]^2 dk. \tag{3.1.19}$$

If we define

$$\beta = \sin\tfrac{1}{2}\theta \tag{3.1.20}$$

so that $m_* = \beta n_*$ from (2.1.13) and use (3.1.16) and (3.1.18), it is tedious, but straightforward, to show that

$$F_0(k_1) = \tfrac{1}{2}\exp\{-k_1^2/2k_*^2\}\int_{k_1}^{\infty} \frac{E(k)}{k}\left\{1 - \left(\frac{k_1}{k}\right)^2\right\}$$
$$\times \exp\{-(k^2 - k_1^2)(1+\beta^2)/4m_*^2\}\, I_0\{(k^2 - k_1^2)(1-\beta^2)/4m^{*2}\}\, dk, \tag{3.1.21}$$

where I_0 is the zeroth-order modified Bessel function of the second kind. Usually $\beta = \sin\frac{1}{2}\theta$ is small since the scattering angle is small.

Pao's form of the spectrum $E(k)$ is given by

$$E(k) = \alpha k^{-\frac{5}{3}} \exp\{-\tfrac{3}{2}\alpha(k\eta)^{\frac{4}{3}}\}, \tag{3.1.22}$$

η is the Kolmogorov microscale defined by $\eta = (\nu^3/\epsilon)^{\frac{1}{4}}$ where ϵ is the rate of dissipation of turbulent energy per unit mass and ν is the kinematic viscosity (Pao 1965). By substituting (3.1.22) into (3.1.21) and letting $\xi = k_1/k$ we have a form suitable for numerical computation:

$$F_0(k_1) = \tfrac{1}{2}\exp\{-k_1^2/2k_*^2\}\alpha k_1^{-\frac{5}{3}}\int_0^1 (1-\xi)^2\,\xi^{\frac{2}{3}} \exp\{-\tfrac{3}{2}\alpha(k_1\eta/\xi)^{\frac{4}{3}}\}$$
$$\times \exp\{-[k_1^2(1-\xi^2)(1+\beta^2)/4m_*^2\xi^2]\}\, I_0[k_1^2(1-\xi^2)(1-\beta^2)/4m_*^2\xi^2]\, d\xi. \tag{3.1.23}$$

Non-dimensionalizing by the Kolmogorov variables ϵ and ν we have

$$\left.\begin{aligned} k_1\eta = \tilde{k}_1, \quad m_*\eta = \tilde{m}_*, \quad \eta = (\nu^3/\epsilon)^{\frac{1}{4}}, \\ [(\epsilon^{\frac{1}{4}}\nu^{\frac{1}{4}})]^{-1} F(k_1) = \tilde{F}(\tilde{k}_1). \end{aligned}\right\} \tag{3.1.24}$$

$\tilde{F}_0(\tilde{k}_1)$ has been computed from (3.1.23) and is shown in figure 3 for several values of $\tilde{m}_*$ where $\beta = 0{\cdot}145$. The true spectrum $\tilde{F}_{11}^1(\tilde{k}_1)$ is also shown for comparison. It is clear that, when $\tilde{k}_1$ becomes of order $\tilde{m}_*$, the spectrum shows significant attenuation. The degree of attenuation is shown more clearly in figure 4, where the velocimeter transfer function defined by $F_0(k_1)/F_{11}^1(k_1)$ has been plotted for several values of $\tilde{m}_*$, with $\beta = 0{\cdot}145$, which corresponds to $\frac{1}{2}\theta \sim 8\frac{1}{2}°$. Figure 5 plots the wavenumber at which the spectrum is reduced to half its true value (the half-power point) as a function of $\tilde{m}_*$ for values of $\beta = 0{\cdot}0725$, $0{\cdot}145$ and $0{\cdot}29$ or equivalently $\frac{1}{2}\theta \sim 4°$, $8\frac{1}{2}°$ and $17°$. The curves are seen to be approximately linear on a log–log plot; clearly, the dependence on angle is diminishing as the angle becomes smaller.

In order to illustrate more clearly the effect of the attenuation at high wavenumbers the true and measured rates of dissipation, say D_T and D_m, were computed from

$$\frac{D_m}{D_T} = \int_{-\infty}^{\infty} k_1^2 F_0(k_1)\, dk_1 \Big/ \int_{-\infty}^{\infty} k_1^2 F_{11}^1(k_1)\, dk_1. \tag{3.1.25}$$

D_m/D_T is shown in figure 6 as a function of $\tilde{m}_*$. It is obvious from the graph that,

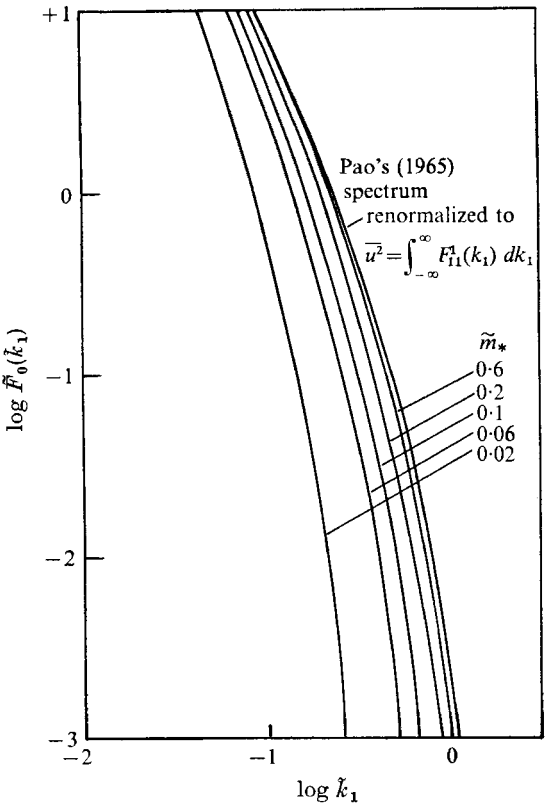

FIGURE 3. Measured spectra computed from (3.1.23), $\alpha = 1{\cdot}7$.

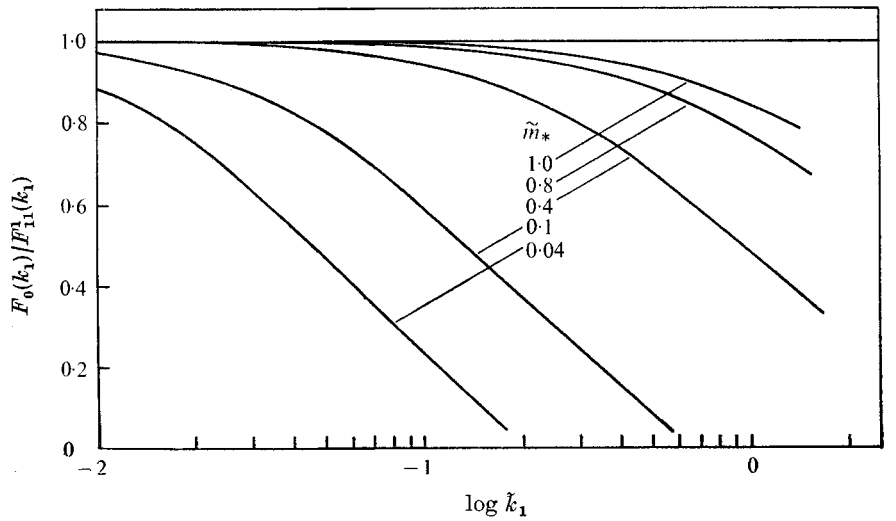

FIGURE 4. Velocimeter transfer function.

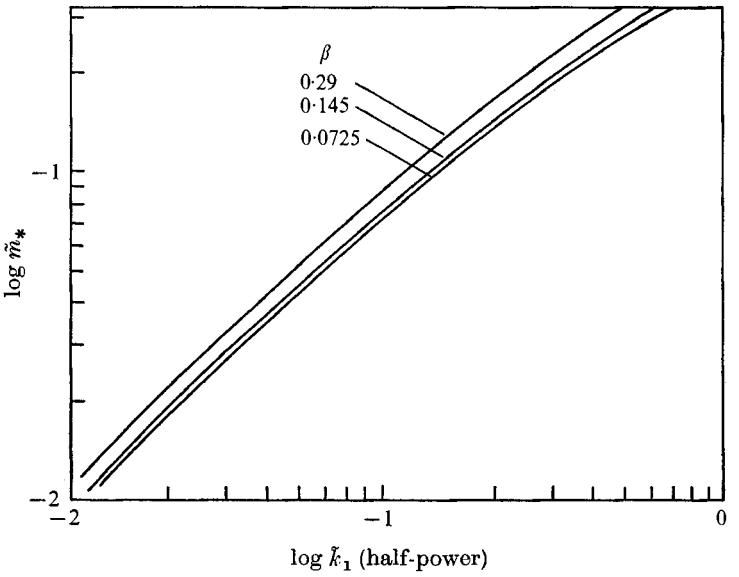

FIGURE 5. Half-power points of velocimeter transfer function.

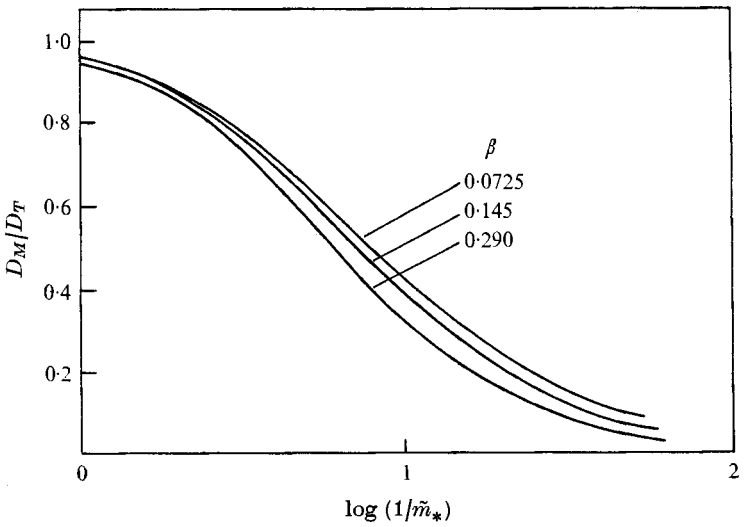

FIGURE 6. Ratio of measured to true turbulent energy dissipation.

if the dissipation is to be measured to 10 % accuracy, $\tilde{m}_*$ must be nearly unity; that is, the largest dimension of the scattering volume must be at least as small as the Komogorov microscale. These results are similar to those obtained by Wyngaard (1968) for a hot wire and may easily be extended to the measurement of cross-stream velocity components.

The analysis of this section would be incomplete without a discussion of the assumptions which were made regarding the character of the turbulence, namely, incompressibility, homogeneity, stationarity and isotropy. This situation is, of course, dynamically impossible; however, as long as the size of the scattering

volume and the passage time of the particles through the scattering volume are very much smaller than the length and time scales characteristic of the turbulence evolution, and the Reynolds number is large, these assumptions are approximately fulfilled and the analysis is valid.

3.2. *Velocity deviations across the scattering volume*

Because of the finite dimensions of the scattering volume, velocity gradients will exist across it. The mean-square velocity deviation at any point in the scattering volume is defined by

$$\overline{[U[\mathbf{x}(\mathbf{a},t),t]-u_0(t)]^2}. \tag{3.2.1}$$

It is simple to show that the average mean-square velocity deviation is given by

$$\overline{\Delta u^2} = \overline{U'^2(\mathbf{a},t)} - \overline{u_0'(t)^2}. \tag{3.2.2}$$

Under the assumptions of incompressibility, homogeneity, stationarity and isotropy it follows immediately from (3.1.4) that

$$\overline{\Delta u^2} = \int_{\mathbf{k}} \Phi_{11}(\mathbf{k})\{1-\mathscr{W}(\mathbf{k})\}\,d\mathbf{k}. \tag{3.2.3}$$

From (3.1.14) and (3.1.16) we have

$$\overline{\Delta u^2} = \int_{-\infty}^{\infty} [F_{11}^1(k_1) - F_0(k_1)]\,dk_1, \tag{3.2.4}$$

which may be computed as a function of (k_*, m_*, n_*) as in (3.1.23).

More physical insight may be gained, however, by relating $\overline{(\Delta u)^2}$ to the rate of dissipation ϵ. By expanding the exponential of (3.2.3) in powers of k_1/k_*, k_2/m_* and k_3/n_* and assuming that $k_*, m_*, n_* \geqslant 0{\cdot}2\eta^{-1}$ (the peak of the dissipation spectrum) we may neglect terms of order greater than two to obtain

$$\overline{(\Delta u)^2} \simeq \tfrac{1}{2}k_*^{-2}\int_{-\infty}^{\infty} k_1^2 F_{11}^1(k_1)\,dk_1 + \tfrac{1}{2}m_*^{-2}\int_{-\infty}^{\infty} k_2^2 F_{11}^2(k_2)\,dk_2 + \tfrac{1}{2}n_*^{-2}\int_{-\infty}^{\infty} k_3^2 F_{11}^3(k_3)\,dk_3. \tag{3.2.5}$$

Assuming isotropy, from Batchelor (1960, p. 45) we may write (3.2.5) as

$$\overline{(\Delta u)^2} \simeq \left(\frac{\epsilon}{15\nu}\right)\left[\frac{1}{2k_*^2}+\frac{1}{m_*^2}+\frac{1}{n_*^2}\right]. \tag{3.2.6}$$

Using the definitions of k_*, m_* and n_* we may write

$$\overline{(\Delta u)^2} = \left(\frac{\epsilon}{15\nu}\right)\left[\frac{1}{m_*^2}\right]\left[1+\sin^2\tfrac{1}{2}\theta\left\{\frac{1+2\cos\frac{1}{2}\theta}{2\cos^2\frac{1}{2}\theta}\right\}\right], \tag{3.2.7}$$

where θ is the scattering angle.

For a scattering angle of $\theta \sim 12°$, $\sin\frac{1}{2}\theta \sim 0{\cdot}1$ and

$$\sin^2\tfrac{1}{2}\theta\left[\frac{1+2\cos\frac{1}{2}\theta}{2\cos^2\frac{1}{2}\theta}\right] \sim 0{\cdot}015.$$

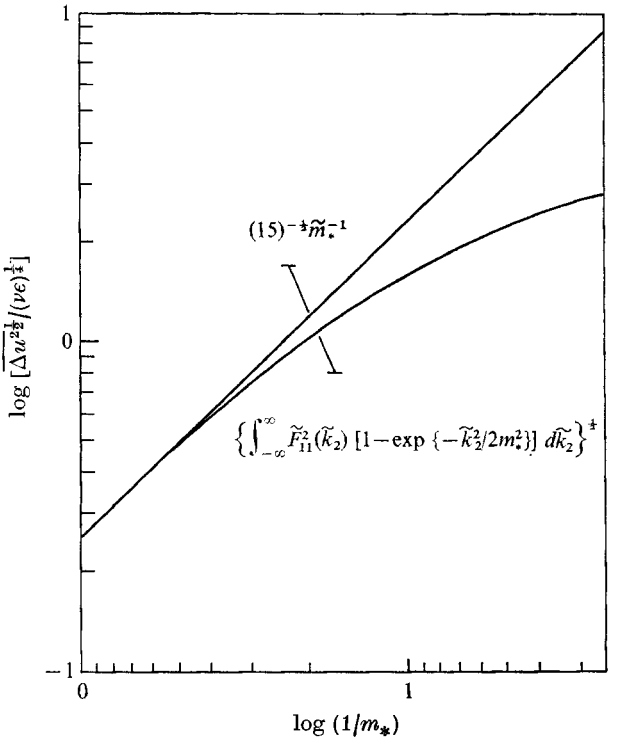

FIGURE 7. Root-mean-square velocity deviation within the scattering volume.

Thus for a small scattering angle

$$\overline{(\Delta u)^2} \simeq \left(\frac{\epsilon}{15\nu}\right)\left[\frac{1}{m_*^2}\right]. \tag{3.2.8}$$

From (3.2.8) and (3.1.2) we may write

$$[\overline{(\Delta u)^2}]^{\frac{1}{2}} = (15)^{-\frac{1}{2}}(\nu\epsilon)^{\frac{1}{4}}\tilde{m}_*^{-1}. \tag{3.2.9}$$

We recognize $(\nu\epsilon)^{\frac{1}{4}}$ as the velocity scale associated with the dissipative turbulent eddies. Thus, if the turbulence does not change, the root-mean-square deviation from the volume-averaged velocity is seen to increase linearly with the largest dimension of the scattering volume. This is consistent with what one might have expected intuitively.

Since k_* and n_* are almost always much larger than m_* and generally chosen near η^{-1}, where the spectrum is falling off very rapidly, another approximation to (3.2.3) may be obtained by ignoring the effect of k_* and n_* and integrating over k_1 and k_3 to yield

$$\overline{(\Delta u)^2} \simeq \int_{-\infty}^{\infty} F_{11}^2(k_2)\,[1-\exp\{-k_2^2/2m_*^2\}]\,dk_2, \tag{3.2.10}$$

where $F_{11}^2(k_2)$ is the transverse spectrum and is defined by

$$F_{11}^2(k_2) = \int_{-\infty}^{\infty} \Phi_{11}(k_1, k_2, k_3)\,dk_1\,dk_3. \tag{3.2.11}$$

Equation (3.2.10) is useful in estimating $\overline{(\Delta u)^2}$ from experimentally determined spectra where the conditions for the asymptotic estimate of (3.2.9) may not be satisfied or where the Reynolds number may be too low to permit an accurate determination from Pao's spectrum as in (3.2.4). Clearly (3.2.10) reduces to (3.2.9) when $m_* \eta \gg 0{\cdot}2$.

The dimensionless root-mean-square velocity deviation $\overline{(\Delta u)^2}^{\frac{1}{2}}/(\nu\epsilon)^{\frac{1}{4}}$ has been plotted as a function of $\tilde{m}_*$ in figure 7. Values obtained numerically using Pao's spectrum in (3.2.10) and (3.2.4) with $\beta = 0{\cdot}145$ coincided to within 5% and were plotted together. The asymptotic estimate of (3.2.9) is seen to be accurate to within 10% when $\tilde{m}_* > 0{\cdot}3$; for values less than this it significantly overestimates the turbulent deviations as would be expected from the shape of the spectrum.

It should be emphasized that $\overline{(\Delta u)^2}$ includes only fluctuations about the volume-averaged velocity $u_0(t)$ and does not include the fluctuations of $u_0(t)$ in time, which must be considered separately as in § 3.1.

4. The total Doppler broadening

4.1. *The correlation* $\overline{i(t)\,i(t')}$

The total Doppler current was seen to be given by (2.3.2). We define $\hat{X}$ as the effective displacement due to $\overline{u_0(t)}$, that is,

$$\hat{X}(t) = \int_0^t \overline{u_0(t_1)}\, dt_1 = \bar{u}t. \tag{4.1.1}$$

By taking the probability densities of the turbulent displacements to be Gaussian, we may write

$$P[X(t)-\hat{X}(t), X(t')-\hat{X}(t')] = \frac{1}{(2\pi)^{\frac{1}{2}}\sigma_x} \exp\{-[(X(t)-\hat{X}(t))-(X(t')-\hat{X}(t'))]^2/2\sigma_x^2\}, \tag{4.1.2}$$

$$P[\Delta(\mathbf{a},t), \Delta(\mathbf{a},t')] = \frac{1}{(2\pi)^{\frac{1}{2}}\sigma_\Delta} \exp\{-[\Delta(\mathbf{a},t)-\Delta(\mathbf{a},t')]^2/2\sigma_\Delta^2\}, \tag{4.1.3}$$

where

$$\sigma_x^2 = \overline{[X(t)-\hat{X}(t)-X(t')+\hat{X}(t')]^2} = \int_0^t\int_0^{t'} \overline{[u_0(t_1)-\bar{u}_0(t_1)]\,[u_0(t_2)-\bar{u}_0(t_2)]}\, dt_1\, dt_2$$
$$= \overline{2u'^2}(t-t')\int_0^{t-t'}\left[1-\frac{x}{t-t'}\right]\rho(x)\,dx$$
$$\simeq \overline{u'^2}(t-t') \text{ for small times} \tag{4.1.4}$$

and

$$\sigma_\Delta^2 = \overline{[\Delta(\mathbf{a},t)-\Delta(\mathbf{a},t')]^2} = \int_0^t\int_0^{t'} \overline{[U(\mathbf{a},t_1)-u_0(t_1)]\,[U(\mathbf{a},t_2)-u_0(t_2)]}\, dt_1\, dt_2$$
$$= \overline{2(\Delta u)^2}\,(t-t')\int_0^{t-t'}\left[1-\frac{x}{t-t'}\right]\rho_0(x)\,dx$$
$$\simeq \overline{(\Delta u)^2}\,(t-t')^2 \text{ for small times.} \tag{4.1.5}$$

Since the turbulence is assumed homogeneous, incompressible, stationary and isotropic, and since the $g(\mathbf{a})$ are statistically independent for different values of the argument, we may compute the $i(t)\,i(t')$ correlation in a straightforward manner using (2.3.2), (4.1.2) and (4.1.3). We have

$$\frac{\overline{i(t)\,i(t')}}{\overline{i^2(t)}} = \exp\left\{-\left(\frac{K^2\sigma_\Delta^2}{2}+\frac{(\hat{X}-\hat{X}')^2}{4\sigma_1^2}\right)\Big/\left(1+\frac{\sigma_x^2}{2\sigma_1^2}+\frac{\sigma_\Delta^2}{2\sigma_1^2}\right)\right\}$$
$$\times\exp\left\{-K^2\sigma_x^2/2\left(1+\frac{\sigma_x^2}{2\sigma_1^2}+\frac{\sigma_\Delta^2}{2\sigma_1^2}\right)\right\}\cos\left\{K(\hat{X}-\hat{X}')\Big/\left(1+\frac{\sigma_x^2}{2\sigma_1^2}+\frac{\sigma_\Delta^2}{2\sigma_1^2}\right)\right\}. \quad (4.1.6)$$

From (2.3.5) we may also write

$$\overline{i(t)\,i(t')} = \overline{F(t)\,F(t')\cos KX\cos KX'}+\overline{G(t)\,G(t')\sin KX\sin KX'}$$
$$+\overline{F(t)\,G(t')\cos KX\sin KX'}+\overline{F(t')\,G(t)\cos KX'\sin KX}. \quad (4.1.7)$$

Following the same procedure as was used to derive (4.1.6), it may be shown that to order $\exp\{-K^2\sigma_1^2\}$, where $K^2\sigma_1^2 \gg 1$, that

$$\overline{F(t)\,F(t')} \simeq \overline{G(t)\,G(t')} \quad (4.1.8)$$

and

$$\overline{F(t)\,G(t')} \simeq 0. \quad (4.1.9)$$

In fact,

$$\frac{\overline{F(t)\,F(t')}}{\overline{F^2(t)}} \simeq \exp\left\{-\left(\frac{K^2\sigma_\Delta^2}{2}+\frac{(\hat{X}-\hat{X}')^2}{4\sigma_1^2}\right)\Big/\left(1+\frac{\sigma_x^2}{2\sigma_1^2}+\frac{\sigma_\Delta^2}{2\sigma_1^2}\right)\right\}$$
$$\times\exp\left\{-K^2\sigma_x^2\left(\frac{\sigma_\Delta^2}{2\sigma_1^2}\right)\Big/\left(1+\frac{\sigma_x^2}{2\sigma_1^2}+\frac{\sigma_\Delta^2}{2\sigma_1^2}\right)\right\}\cos\left\{K(\hat{X}-\hat{X}')\left(\frac{\sigma_\Delta^2}{2\sigma_1^2}\right)\Big/\left(1+\frac{\sigma_\Delta^2}{2\sigma_1^2}+\frac{\sigma_x^2}{2\sigma_1^2}\right)\right\}. \quad (4.1.10)$$

Furthermore,

$$\overline{\cos K(X-X')} = \exp\{-\tfrac{1}{2}K^2\sigma_x^2\}\cos K(\hat{X}-\hat{X}'). \quad (4.1.11)$$

Inspection of (4.1.6)–(4.1.11) reveals that when

$$\frac{\sigma_x^2}{2\sigma_1^2}+\frac{\sigma_\Delta^2}{2\sigma_1^2} \ll 1 \quad (4.1.12)$$

equation (4.1.7) reduces to

$$\overline{i(t)\,i(t')} = \overline{F(t)\,F(t')}\cos\overline{K(X-X')}. \quad (4.1.13)$$

To justify (4.1.12) we note from (4.1.6) that, when

$$K^2\sigma_x^2 \simeq K^2\overline{u'^2}(t-t')^2 \gg 1, \quad (4.1.14)$$

the correlation $\overline{i(t)\,i(t')} \simeq 0$. Hence, we need only concern ourselves with times of order

$$T \sim 1/2^{\frac{1}{2}}Ku'. \quad (4.1.15)$$

It follows that

$$\frac{\sigma_x^2}{2\sigma_1^2} \sim \frac{1}{4}\frac{1}{K^2\sigma_1^2} \ll 1, \quad (4.1.16)$$

$$\frac{\sigma_\Delta^2}{2\sigma_1^2} \sim \frac{1}{4}\frac{\overline{(\Delta u)^2}}{u'^2}\frac{1}{K^2\sigma_1^2} < \frac{\sigma_x^2}{2\sigma_1^2}. \quad (4.1.17)$$

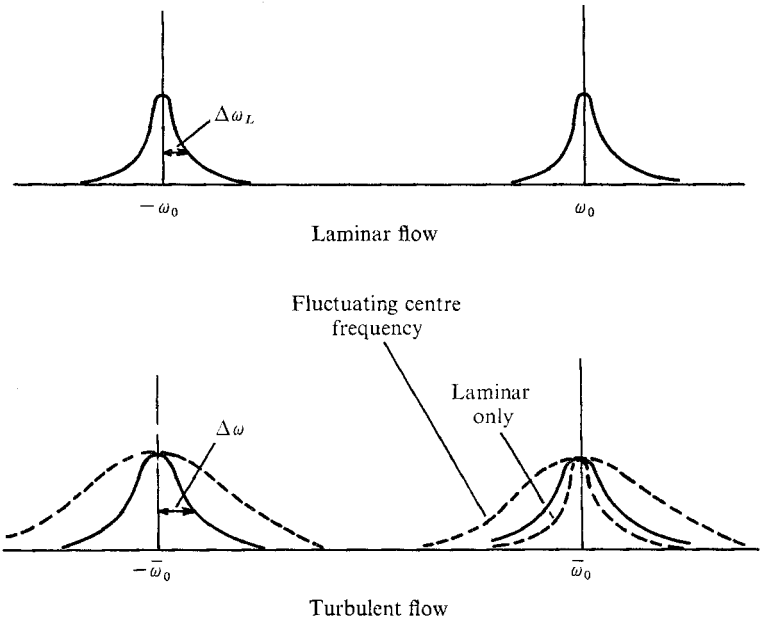

FIGURE 8. Spectrum of the Doppler signal current.

Hence to order $\exp\{-K^2\sigma_1^2\}$, where $K^2\sigma_1^2 \gg 1$, we have

$$\frac{\overline{i(t)\,i(t')}}{\overline{i^2(t)}} = \exp\left\{-\frac{K^2\sigma_\Delta^2}{2} + \frac{(\hat{X}-\hat{X}')^2}{4\sigma_1^2}\right\} \exp\{-\tfrac{1}{2}K^2\sigma_x^2\} \cos K(\hat{X}-\hat{X}') \tag{4.1.18}$$

and

$$\frac{\overline{F(t)\,F(t')}}{\overline{F^2(t)}} = \exp\left\{-\frac{K^2\sigma_\Delta^2}{2} + \frac{(\hat{X}-\hat{X}')^2}{4\sigma_1^2}\right\}. \tag{4.1.19}$$

It is straightforward to show that the effect of the particle meandering in the y and z directions is also smaller than $\exp\{-K^2\sigma_1^2\}$ where $K^2\sigma_1^2 \gg 1$.

In summary, we have derived the correlation coefficient for the Doppler current $\overline{i(t)\,i(t')}/\overline{i^2(t)}$ and for $\overline{F(t)\,F(t')}/\overline{F^2(t)}$. Moreover, since F and G are Gaussian and are therefore completely determined by their second-order statistics and since X is assumed Gaussian, we have from (4.1.19) that the fluctuations of F and G are statistically independent of the fluctuations of $X(t)$, a fact of major importance since the centre frequency fluctuations may be treated separately from the ambiguities.

4.2. *The spectrum of the Doppler current*

From (4.1.13), we have

$$\frac{\overline{i(t)\,i(t+\tau)}}{\overline{i^2(t)}} = \frac{\overline{F(t)\,F(t+\tau)}}{\overline{F^2(t)}} \overline{\cos K[X(t)-X(t+\tau)]}. \tag{4.2.1}$$

Let

$$\hat{F}(\omega) = \mathscr{F}\{\overline{F(t)\,F(t+\tau)}/\overline{F^2(t)}\} \tag{4.2.2}$$

and

$$\hat{G}(\omega) = \mathscr{F}\{\overline{\cos K[X(t)-X(t+\tau)]}\}, \tag{4.2.3}$$

where $\mathscr{F}$ denotes the Fourier transform. The spectrum of the current is then given by

$$I(\omega) = \mathscr{F}\{\overline{i(t)\,i(t+\tau)}/\overline{i^2(t)}\} \tag{4.2.4}$$

or using (4.2.1)

$$I(\omega) = \hat{F}(\omega) * \hat{G}(\omega) = \int_{-\infty}^{\infty} \hat{F}(\omega_1)\,\hat{G}(\omega-\omega_1)\,d\omega_1, \tag{4.2.5}$$

where $*$ denotes a convolution and we have used Parseval's relation. It is easy to show that

$$\hat{F}(\omega) = \exp\{-\omega^2/2(\Delta\omega)^2\}, \tag{4.2.6}$$

where

$$(\Delta\omega)^2 = (\Delta\omega_T)^2 + (\Delta\omega_L)^2, \tag{4.2.7}$$

$$(\Delta\omega_L)^2 = \overline{u}^2/2\sigma_1^2 = (k_*\,\overline{u})^2, \tag{4.2.8}$$

$$(\Delta\omega_T)^2 = K^2\overline{(\Delta u)^2}, \tag{4.2.9}$$

and that

$$\hat{G}(\omega) = \exp\{-(\omega-\overline{\omega}_0)^2/2(\Delta\omega_{u_0})^2\} + \exp\{-(\omega+\overline{\omega}_0)^2/2(\Delta\omega_{u_0})^2\}, \tag{4.2.10}$$

where

$$\overline{\omega}_0 = K\overline{u_0} \tag{4.2.11}$$

and

$$(\Delta\omega_{u_0})^2 = K^2\overline{u_0'^2}. \tag{4.2.12}$$

Hence the spectrum of the Doppler current is given by

$$I(\omega) = \exp\{-(\omega-\overline{\omega}_0)^2/2(\Delta\omega^2+\Delta\omega_{u_0}^2)\} + \exp\{-(\omega+\overline{\omega}_0)^2/2(\Delta\omega^2+\Delta\omega_{u_0}^2)\}. \tag{4.2.13}$$

Thus the spectrum consists of Gaussian peaks centred at $\pm\overline{\omega}_0$ and is shown in figure 8 for laminar and turbulent flow.

It is clear that, when there is no turbulence, the total Doppler bandwidth is given by

$$\Delta\omega = \Delta\omega_L.$$

In a turbulent flow, however, the turbulence contributes to the Doppler broadening in two distinct ways: first, through the broadening due to variations in velocity across the scattering volume, $\Delta\omega_T$; and, second, through the fluctuations of the volume-averaged velocity, $\Delta\omega_{u_0}$. It should be noted that, because of the Gaussian model used for both the volume-averaged velocity and the velocity variations across the scattering volume, the latter, $\overline{(\Delta u)^2}$, merely serves to restore the attenuated part of $\overline{u'^2}$ to $\overline{u_0'^2}$. This unfortunately does not appear to be true in general and the two types of broadening contribute in distinct and separate ways to the total broadening.

Other factors may contribute to an ambiguous broadening of the Doppler spectrum such as gradients of mean velocity across the scattering volume, the Brownian motion of the scattering particles and a non-monochromatic light source (cf. Edwards *et al.* 1971). If these effects were Gaussian in nature, the total Doppler bandwidth could be given by

$$(\text{Bandwidth})^2 = \Delta\omega_{u_0}^2 + \Delta\omega_T^2 + \Delta\omega_L^2 + \Delta\omega_G^2 + \Delta\omega_\beta^2 + \Delta\omega_s^2, \tag{4.2.14}$$

where $\Delta\omega_G$, $\Delta\omega_\beta$ and $\Delta\omega_s$ represent mean velocity gradient, Brownian motion and source broadening respectively. We shall ignore these effects in the remainder of this paper.

Borrowing a term from RADAR terminology, we shall call $\Delta\omega$, the Doppler broadening rising from sources other than the fluctuations of the centre frequency, the Doppler ambiguity.

4.3. *Measurement of turbulent intensities from the spectrum*

Since the envelope of the Doppler current spectrum is dependent on the probability density of the integral $X(t)$ of the velocity field $u_0(t)$, we may attempt to derive information about the turbulent velocities by examining the spectrum. When the probability density of $X(t)$ is Gaussian, we have seen that the total Doppler broadening is proportional to the root-mean-square turbulence velocity $(\overline{u'^2})^{\frac{1}{2}}$. The foregoing analysis must be taken into consideration whenever one attempts to measure mean-square fluctuating quantities from the spectrum of the Doppler signal. When the fluctuations of ω_0 are of order $\Delta\omega$, the fluctuating velocities can no longer be distinguished from the fluctuations due to the Doppler ambiguity. The problem is illustrated graphically in figure 8. The limit of resolution may be taken as

$$\Delta\omega/\overline{\omega}_0 < u'/\overline{u}. \tag{4.3.1}$$

It should be noted that, because of the broadening $\Delta\omega_T$ due to turbulent velocity variation, the intensity values measured from the spectral broadening may not be corrected by simply subtracting the values measured in laminar flow as suggested by some authors (Pike *et al.* 1967; Goldstein & Kreid 1967). Failure to account properly for the Doppler ambiguity may explain the anomalous results of Greated (1969).

5. The instantaneous signal

5.1. *The spectrum of* ω_1

The output from a typical FM detector was given by (2.3.9) as

$$\omega_1 = Ku_0(t) - \dot{\phi}.$$

Assuming that Taylor's hypothesis is valid in the flow under consideration, we may write

$$u_0(t) = \int_{-\infty}^{\infty} e^{i\alpha t}\, dZ(\alpha), \quad \overline{dZ(\alpha)\, dZ^*(\alpha')} = \begin{cases} 0, & \alpha \neq \alpha', \\ F_0(\alpha/\overline{u})\, d\alpha/\overline{u}, & \alpha = \alpha', \end{cases} \tag{5.1.1}$$

$$\dot{\phi} = \int_{-\infty}^{\infty} e^{i\alpha t}\, dN_1(\alpha), \quad \overline{dN_1(\alpha)\, dN_1^*(\alpha')} = \begin{cases} 0, & \alpha \neq \alpha', \\ N(\alpha)\, d\alpha, & \alpha = \alpha', \end{cases} \tag{5.1.2}$$

where F_0 is the spectrum of u_0 and N is the spectrum of the phase fluctuations. Substituting into (2.3.8), we have

$$\omega_1 = K\int_{-\infty}^{\infty} e^{i\alpha t}\, dZ(\alpha) - \int_{-\infty}^{\infty} e^{i\alpha t}\, dN_1(\alpha). \tag{5.1.3}$$

Since the phase fluctuations and Ku_0 are uncorrelated, the spectrum of ω_1 is given by

$$K^2 F_0(\alpha/\overline{u})/\overline{u} + N(\alpha).$$

The problem of measuring turbulent spectra has thus been reduced to 'what is $N(\alpha)$?'

5.2. *The nature of the phase fluctuations*

Since F and G are identically distributed Gaussian random variables, we may take F and G to be the co-ordinates of a point in the x, y plane, which moves in such a way that it has a circularly symmetric Gaussian distribution. ϕ is the angle subtended by the radius vector to the point and the x axis.

It is evident that ϕ is not stationary. If ϕ begins from zero, say, then for times short compared with $2\pi/\Delta\omega$ the probability of finding $|\phi| > 2\pi$ will be small; as time passes it becomes more and more likely that ϕ will have made one or more revolutions about the origin. If $\dot{\phi}(t)$ is stationary,

$$\phi(t) = \phi(0) + \int_0^t \dot{\phi}(t')\,dt', \tag{5.2.1}$$

$$\overline{\phi(t)\,\phi(t)} = \overline{\phi(t)\,\phi(0)} + \int_0^t \overline{\dot{\phi}(t)\,\dot{\phi}(t')}\,dt'. \tag{5.2.2}$$

As we let $t \to \infty$, $\overline{\dot{\phi}(t)\,\phi(0)} \to 0$ and

$$\begin{aligned}\frac{d}{dt}\frac{\overline{\phi^2(t)}}{2} &\cong \int_0^\infty \overline{\dot{\phi}(t)\,\dot{\phi}(t')}\,dt' \\ &= \int_{-\infty}^0 \overline{\dot{\phi}(t)\,\dot{\phi}(t+\tau)}\,d\tau, \quad t'-t=\tau, \\ &= \frac{1}{2}\int_{-\infty}^{+\infty} \overline{\dot{\phi}(t)\,\dot{\phi}(t+\tau)}\,d\tau,\end{aligned} \tag{5.2.3}$$

since the correlation is symmetric. Hence, the value of the spectrum at the origin is given by

$$N(0) = \frac{1}{2\pi}\int_{-\infty}^{\infty} \overline{\dot{\phi}(t)\,\dot{\phi}(t+\tau)}\,d\tau = \frac{1}{2\pi}\frac{d\overline{\phi^2}}{dt}. \tag{5.2.4}$$

This clearly will be non-zero since ϕ is non-stationary.

The joint characteristic functional of F and G is determined entirely by one parameter $\Delta\omega$; consequently, that of $\dot{\phi}$ will also be determined only by $\Delta\omega$. Hence, we must have on dimensional grounds

$$d\overline{\phi^2}/dt \propto \Delta\omega \tag{5.2.5}$$

with an unknown coefficient, hopefully of order unity.

5.3. *An exact expression for the correlation* $\overline{\dot{\phi}(t)\,\dot{\phi}(t+\tau)}$†

It was shown in (2.3.5) that the Doppler current under appropriate restrictions could be represented by

$$i(t) = F(t)\cos KX + G(t)\sin KX,$$

† Earlier presentations of this work (cf. Lumley *et al.* 1969; George 1971) appear to be based on a faulty assumption regarding the correlation of the radial and angular components of the signal. The authors are grateful to Professor N. Berman for calling the work of Rice and others to their attention.

where $X = X(t)$ and F and G are Gaussian random variables. Alternatively

$$i(t) = (F^2+G^2)^{\frac{1}{2}} \cos(KX - \phi),$$

where

$$\tan\phi(t) = G/F.$$

Differentiating we have

$$\dot{\phi}(t) = \frac{d\phi}{dt} = \frac{F\dot{G} - G\dot{F}}{F^2+G^2}. \tag{5.3.1}$$

The correlation $\overline{\dot{\phi}(t)\,\dot{\phi}(t+\tau)}$ is then given by

$$R_N(\tau) = \overline{\left(\frac{G_1\dot{F}_1 - F_1\dot{G}_1}{F_1^2+G_1^2}\right)\left(\frac{G_2\dot{F}_2 - F_2\dot{G}_2}{F_2^2+G_2^2}\right)}, \tag{5.3.2}$$

where the indices 1 and 2 refer to the two time points t and $t+\tau$ and where ensemble averages have to be performed using the joint probability density of the eight variables F_1, G_1, $\dot{F}_1$, $\dot{G}_1$, F_2, G_2, $\dot{F}_2$ and $\dot{G}_2$. This probability density is an eight-dimensional Gaussian distribution and the problem is identical to that of filtered noise detection in an FM receiver (cf. Lawson & Uhlenbeck 1950; Rice 1948; Middleton 1950). The correlation of the random phase fluctuations may be shown to be given by (Lawson & Uhlenbeck 1950, p. 373)

$$R_N(\tau) = \frac{1}{2}\left(\frac{\ddot{\rho}}{\rho} - \frac{\dot{\rho}^2}{\rho^2}\right)\log(1-\rho^2), \tag{5.3.3}$$

where

$$\rho(\tau) = \overline{F(t)\,F(t+\tau)}/\overline{F^2} = \overline{G(t)\,G(t+\tau)}/\overline{G^2}. \tag{5.3.4}$$

Of particular interest is the fact that $R_N(\tau)$ becomes logarithmically infinite as $\tau \to 0$. This may be explained physically by noting that, since the displacement in one direction and velocity in the orthogonal direction (of the point moving on the plane) are independent, arbitrarily large values of the *angular* velocity $\dot{\phi}$ can occur, corresponding to a finite linear velocity and arbitrarily small (orthogonal) displacement. As a consequence of this behaviour, any attempt to measure turbulent energy $\overline{u^2}$ by averaging the squared output signal is rendered futile since

$$\overline{\omega_1^2} = K^2\overline{u^2} + \overline{\dot{\phi}^2} \tag{5.3.5}$$

and $\overline{\dot{\phi}^2} = \infty$.

We have already shown that F and G have Gaussian correlation functions

$$\rho(\tau) = \exp\{-\tfrac{1}{2}(\Delta\omega)^2\tau^2\}. \tag{5.3.6}$$

The corresponding $R_N(\tau)$ is then given by

$$R_N(\tau) = -\tfrac{1}{2}(\Delta\omega)^2\log(1-\rho^2) \tag{5.3.7}$$

and is shown in figure 9. Recall that this will be added to the correlation of the turbulence and will render the measurement of microscales difficult at best, if not impossible.

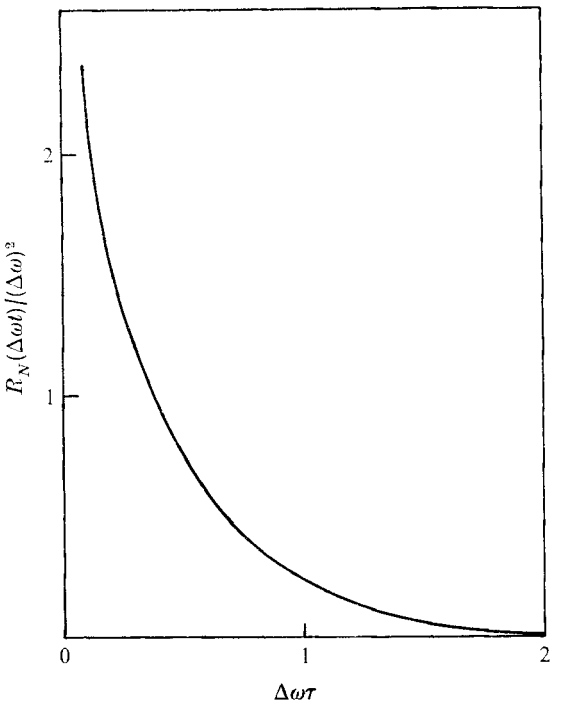

FIGURE 9. Autocorrelation $R_N(\tau)$ of the phase fluctuations.

$$R_N(\tau) \equiv \overline{\dot{\phi}(t)\,\dot{\phi}(t+\tau)} = \frac{1}{2}\left(\frac{\ddot{\rho}}{\rho} - \frac{\dot{\rho}^2}{\rho}\right) \log(1-\rho^2), \quad \rho(\tau) = \exp[-\tfrac{1}{2}(\Delta\omega\tau)^2].$$

5.4. *The spectrum of the random phase fluctuations*

Substitution of (5.3.6) into (5.3.3), expansion of the logarithms in powers of ρ^2 and Fourier transformation term by term gives the following form for the spectrum† (cf. Rice 1948):

$$N(\alpha) = \frac{1}{4\pi^{\frac{1}{2}}}\Delta\omega \sum_{n=1}^{\infty} n^{-\frac{3}{2}} \exp\left\{-\frac{\alpha^2}{4n(\Delta\omega)^2}\right\}. \tag{5.4.1}$$

As long as $\alpha < \Delta\omega$, the effect of the exponential is small and

$$N(\alpha) \simeq N(0) \quad (\alpha < \Delta\omega). \tag{5.4.2}$$

We may approximate (5.4.1) by a finite sum and a remainder as

$$N(\alpha) \simeq \frac{1}{4\pi^{\frac{1}{2}}}\Delta\omega\left(\sum_{n=1}^{M-1} n^{-\frac{3}{2}} \exp\left\{-\frac{\alpha^2}{4n(\Delta\omega)^2}\right\} + \frac{2\pi^{\frac{1}{2}}\Delta\omega}{\alpha}\operatorname{erf}\left[\frac{\alpha}{2M^{\frac{1}{2}}\Delta\omega}\right]\right), \tag{5.4.3}$$

where the last term was obtained by writing the remainder as an integral from M to ∞. By choosing $M = \alpha^2/4(\Delta\omega)^2$ and letting $\alpha \to \infty$, we have

$$N(\alpha) \simeq (\Delta\omega)^2/2\alpha \quad (\alpha \gg \Delta\omega). \tag{5.4.4}$$

This result is also obvious from the logarithmic singularity of the correlation at the origin.

† Spectra are defined on the whole line $(-\infty, \infty)$.

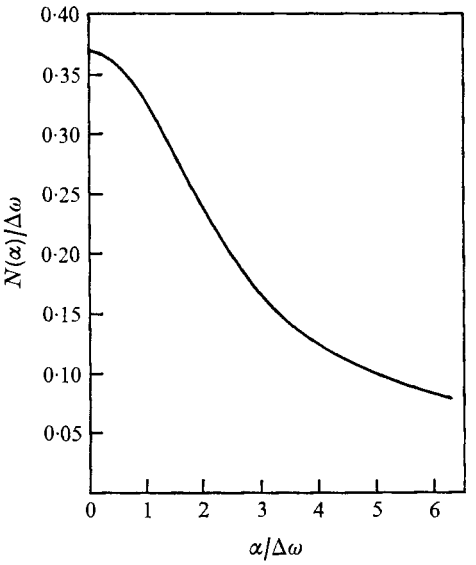

FIGURE 10. Spectrum of the phase fluctuations, adapted from Rice (1948) (normalized on whole line).

The spectrum was calculated from (5.4.3) by Rice (1948) for $M = 12$ and his spectrum is shown in figure 10.

Usually $\alpha \sim \Delta\omega$ represents a frequency well above the highest turbulence frequency of interest and the spectrum is experimentally white. Therefore, to simplify the analysis in the remainder of this paper, we shall approximate the spectrum of the random phase fluctuation by its value at the origin, that is

$$N(0) = 0{\cdot}368\Delta\omega \quad (\alpha < \Delta\omega). \tag{5.4.5}$$

5.5. *The limit of spectral measurement*

The limit of measurement of $F_{11}(\alpha)$ will be determined by the frequency α_0 where the ratio of the turbulence spectrum to the ambiguity spectrum is unity, or where

$$(K^2/\overline{u})\, F_{11}^1(\alpha_0/\overline{u}) = N(\alpha_0). \tag{5.5.1}$$

Non-dimensionalizing by Kolmogorov variables ϵ and ν we have, using (4.2.7) for $\Delta\omega$ and the asymptotic estimate for $\Delta\omega_T$ given in equation (3.2.9),

$$\tilde{F}_{11}^1(\tilde{k}_0) = 9{\cdot}33 \times 10^{-3} \tilde{k}_* R^2 \left\{1 + \frac{(2\pi)^2}{15R^2\tilde{k}_*^4 \sin^2 \tfrac{1}{2}\theta}\right\}^{\frac{1}{2}}, \tag{5.5.2}$$

where

$$\tilde{k}_0 = \alpha_0 \eta/\overline{u}. \tag{5.5.3}$$

The first term represents the effect of the transit time broadening and the second term represents the effect of the turbulence broadening. The parameter R is defined by

$$R = \frac{2\pi}{\nu}\frac{\overline{u}}{K} = \frac{2\pi}{\nu}\frac{\overline{u}^2}{\overline{\omega}_0} = \frac{\overline{u}\lambda}{2\nu \sin \tfrac{1}{2}\theta}. \tag{5.5.4}$$

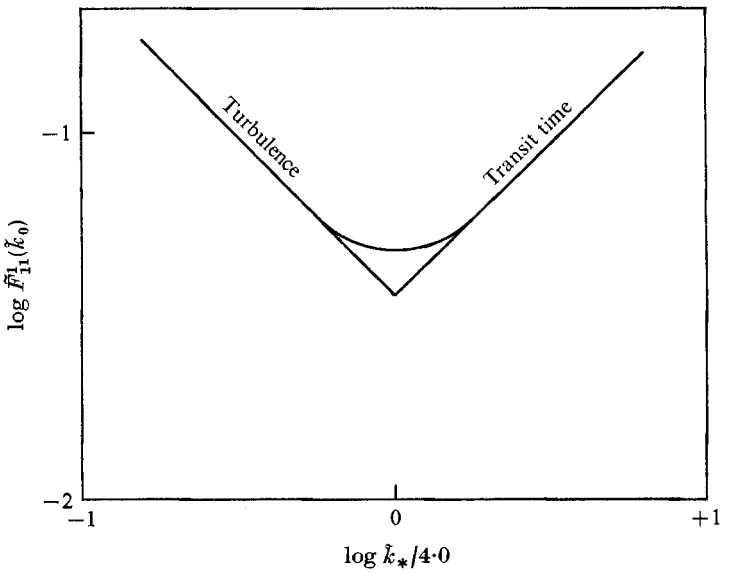

FIGURE 11. Combined transit time and turbulence broadening. $\tilde{F}^1_{11}(\tilde{k}_0)$ defined by (5.5.2); $R = 1{\cdot}0$, $\sin\frac{1}{2}\theta = 0{\cdot}1$, $k_{*\mathrm{opt}} = 4{\cdot}0$.

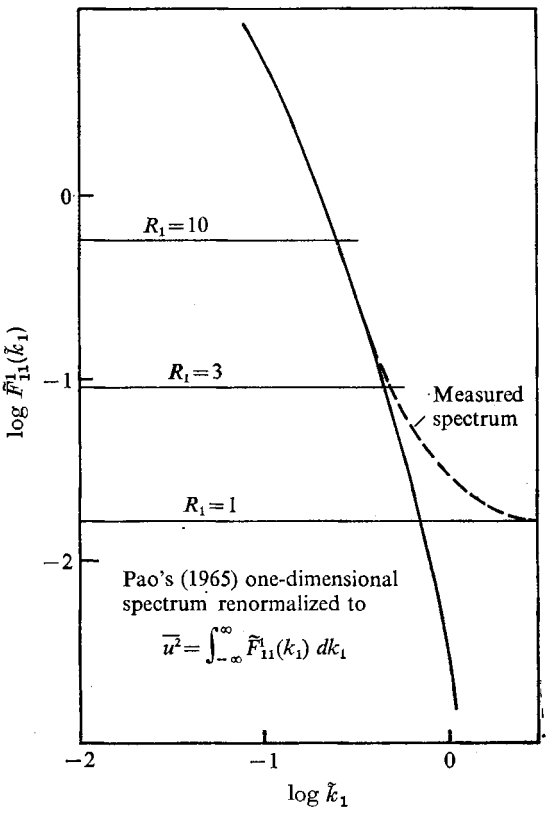

FIGURE 12. Optimum ambiguity spectra. $k_*\eta = 1{\cdot}27(R\sin\frac{1}{2}\theta)^{-\frac{1}{2}}$, $R = \overline{u}\lambda/2\nu\sin\frac{1}{2}\theta$, $R_1 = R/\sin^3\frac{1}{2}\theta$.

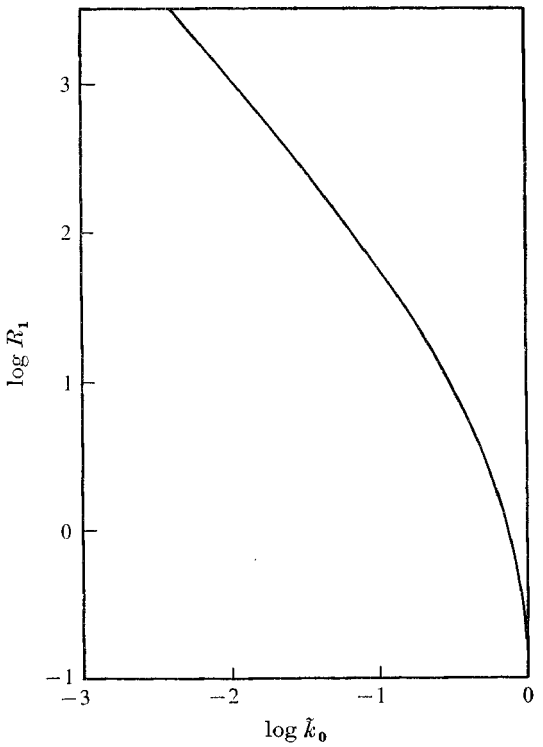

FIGURE 13. Wavenumber corresponding to an ambiguity-to-turbulence ratio of unity under optimum conditions. $\tilde{F}^1_{11}(\tilde{k}_0) = 1{\cdot}68 \times 10^{-2} R_1^{\frac{3}{2}}$, $R = \bar{u}\lambda/2\nu \sin\frac{1}{2}\theta = 2\pi\bar{u}^2/\nu\bar{\omega}_0$, $R_1 = R/\sin^{\frac{1}{3}}\frac{1}{2}\theta$.

Physically, R is just a Reynolds number based on the smallest length that can be resolved in the mean flow direction; if the 'crests' of the light waves (wavelength λ) make an angle $\frac{1}{2}\theta$ with the direction of mean flow, then $\frac{1}{2}\lambda \sin\frac{1}{2}\theta$ is the smallest length that can be resolved in that direction.

The lowest ambiguity spectral level (highest cut-off frequency α_0) is obtained when the contributions of the turbulence and the transit time are equal; from (5.5.2) the optimum cut-off wavenumber is then

$$\tilde{k}_{*\mathrm{opt}} = 1{\cdot}27(R \sin\tfrac{1}{2}\theta)^{-\frac{1}{2}}. \tag{5.5.5}$$

Thus the lowest ambiguity spectral height for fixed R and θ is given by

$$\tilde{F}^1_{11}(\tilde{k}_0) = 1{\cdot}68 \times 10^{-2} R^{\frac{3}{2}}/(\sin\tfrac{1}{2}\theta)^{\frac{1}{2}}. \tag{5.5.6}$$

This equation implicitly determines the largest $\tilde{k}_0$ (the wavenumber for which the ratio of the turbulence to ambiguity spectrum is unity) that can be obtained for fixed R and θ.

The ambiguity spectral levels from (5.5.2) are shown in figure 11; the combined effects of the finite transit time and turbulence broadening are demonstrated as a function of $\tilde{k}_*/\tilde{k}_{*\mathrm{opt}}$ for $R = 1{\cdot}0$ and $\sin\frac{1}{2}\theta = 0{\cdot}1$.

The optimum spectra from (5.5.6) are shown in figure 12 for several values of $R_1 = R/\sin^{\frac{1}{3}}\frac{1}{2}\theta$. Pao's spectrum for the turbulence has also been plotted; $\tilde{k}_0$ is determined by the intersection of the turbulence and ambiguity spectra.

Finally, figure 13 shows $\tilde{k}_0$ as a function of R_1. $\tilde{k}_0$ is determined implicitly by (5.5.6) and Pao's spectrum has been used for $\tilde{F}_{11}^1(\tilde{k}_0)$.

From figure 13 it can be seen that, for $\tilde{k}_0 = 1$, $R/\sin^{\frac{1}{3}}\frac{1}{2}\theta = 0{\cdot}10$. With typical values of $\lambda = 6{\cdot}3 \times 10^{-5}$ cm, $\nu = 10^{-2}$ cm^2/s (corresponding to measurements in water) and $2\sin\frac{1}{2}\theta = 0{\cdot}2$ we have $\bar{u} \cong 1{\cdot}5$ cm/s. Relaxation of the resolution requirements to $\tilde{k}_0 = 0{\cdot}1$ increases the permissible mean velocity $\bar{u}$ by about two orders of magnitude. It should be remembered, however, that the $\tilde{k}_0$ determined from (5.5.6) is actually quite conservative since a turbulence/ambiguity ratio of unity does not permit accurate determination of the spectrum.

From figure 12 it can be seen that, for $\tilde{k}_0 \sim 1$, the spectrum begins to deviate perceptibly at about $\tilde{k}_0 \sim 0{\cdot}5$. A certain amount of subtraction of the ambiguity can be done since it is uncorrelated with the turbulence.

The situation might be improved somewhat by increasing the mean Doppler frequency $\bar{\omega}_0$ which corresponds to increasing the scattering angle θ. Unfortunately, forward scattering is much more efficient and it is difficult in practice to achieve a suitable Doppler signal when $2\sin\frac{1}{2}\theta$ is much above 0·7. Additional problems may arise from the electronics as higher frequencies are used.

5.6. *Intensity measurements and higher order statistics*

We have seen that the mean-square value of $\dot{\phi}$ is infinite. This value in practice is finite because of the low-pass filtering introduced by the detection process; however, considerable contamination of intensity measurements from the instantaneous signal may result because of the wide-band nature of $\dot{\phi}$. Clearly ambiguity contributions will be present and perhaps even dominant in attempts to measure higher order statistics such as skewness and kurtosis.

5.7. *Two-point velocity correlations*

Two-point velocity correlations may be performed using two independent laser-Doppler velocimeters. From (2.3.3) and the fact that F and G are Gaussian it may be shown that the correlation between the phase fluctuations induced by the Doppler ambiguity from the two velocimeters is no greater than

$$\exp\left\{-\frac{r_1^2}{2\sigma_1^2}+\frac{r_2^2}{2\sigma_2^2}+\frac{r_3^2}{2\sigma_3^2}\right\},$$

where (r_1, r_2, r_3) measure the distance between the scattering-volume centres in the (x, y, z) directions respectively. When any one of $r_1, r_2, r_3 \gg \sigma_1, \sigma_2, \sigma_3$ the phase fluctuations are effectively uncorrelated and

$$\begin{aligned}\overline{\omega_1^{(1)}\omega_1^{(2)}} &= \overline{\omega_0^{(1)}\omega_0^{(2)}} + \overline{\dot{\phi}^{(1)}\dot{\phi}^{(2)}} \\ &= \overline{\omega_0^{(1)}\omega_0^{(2)}} \\ &= K^2\overline{u_0^{(1)}u_0^{(2)}},\end{aligned}$$

where (1) and (2) denote the signals from the two velocimeters. This is consistent with the observations of Clark (1970), who successfully measured velocity correlations in turbulent pipe flow by using two velocimeters.

It has been suggested (Morton 1970, private communication) that the phase fluctuations from two velocimeters looking at the same scattering volume might be uncorrelated if the velocimeters were placed at different angles to the flow (i.e. rotated about the axis defined by the mean flow direction) because the phases for individual particles would be different. An examination of (2.2.2) reveals that the phase of a scattering particle depends only on its initial x co-ordinate, which is the same for each velocimeter. Thus, while the correlation may not be unity because of the possibly different amplitudes associated with each particle, it will be significant if the scattering volumes overlap.

6. Summary and conclusions

6.1. *Review of results*

The limitations on the use of a laser-Doppler velocimeter in the measurement of turbulence have been explored theoretically. The relationship between the size of the scattering volume and the resolution of the velocimeter was explored and criteria for accurate measurement were established; briefly, it was found that the turbulent fluctuations of wavenumber larger than the cut-off wavenumber associated with the largest dimension of the scattering volume were seriously attenuated.

The influence of the Doppler ambiguity on the measurement of spectra and other statistical quantities was examined. The Doppler ambiguity was seen to arise primarily from the finite transit time of particles through the scattering volume and velocity fluctuations within the volume. In addition, the effects of a mean velocity gradient, Brownian motion, source non-monochromaticity and electronic noise may be important. The spectrum of the phase fluctuations was seen to be experimentally white and proportional in height to the bandwidth of the Doppler ambiguity. Criteria for minimizing the height of the ambiguity spectrum were established and an optimum scattering-volume cut-off wavenumber for minimization was given as

$$\tilde{k}_{*\mathrm{opt}} = 1{\cdot}27(R\sin\tfrac{1}{2}\theta)^{-\frac{1}{2}}, \tag{6.1.1}$$

where $R = 2\pi\overline{U}^2/\nu\bar{\omega}_0$ and where $\tilde{k}_*$ is the dimensionless cut-off wavenumber associated with the dimension of the scattering volume in the direction of the mean flow.

6.2. *The measurement of spectra*

We must discuss the relationship between the resolution criteria and the criteria for minimizing the Doppler ambiguity.

For small scattering angles, the wavenumber m_* associated with the largest dimension of the scattering volume is related to k_* by

$$m_* \cong k_* \sin\tfrac{1}{2}\theta/\cos\tfrac{1}{2}\theta. \tag{6.2.1}$$

We then have

$$m_{*\mathrm{opt}} = k_{*\mathrm{opt}} \frac{\sin\frac{1}{2}\theta}{\cos\frac{1}{2}\theta} \simeq 1{\cdot}27\left[\frac{\sin\frac{1}{2}\theta}{R}\right]^{\frac{1}{2}}, \tag{6.2.2}$$

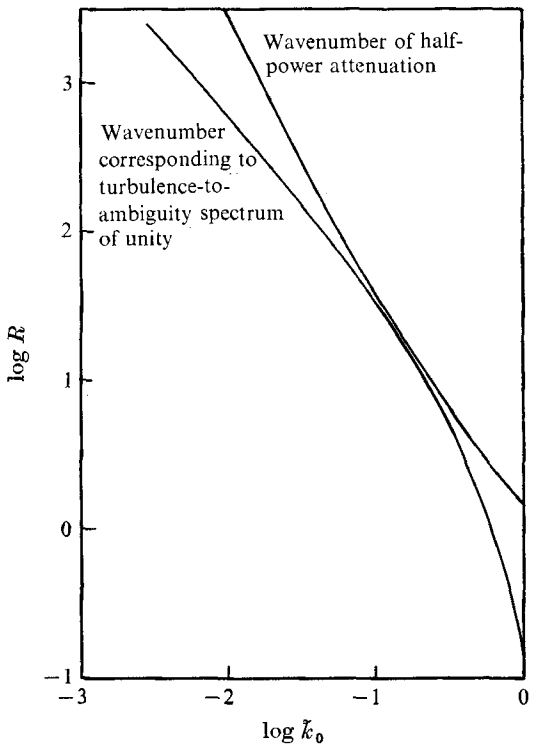

FIGURE 14. Plot of combined ambiguity and spatial resolution cut-off wavenumbers. $\tilde{m}_{*\mathrm{opt}} = 1{\cdot}27[\sin(\frac{1}{2}\theta)/R]^{\frac{1}{4}}$, $\sin\frac{1}{2}\theta = 0{\cdot}145$.

We saw in § 3.1 that $\tilde{m}_*$ determines the half-power point of the spectral transfer function, that is, the wavenumber at which the measured spectrum is attenuated by 50 %. Clearly $\tilde{m}_{*\mathrm{opt}}$ determines the half-power point when the scattering volume is chosen for minimum Doppler ambiguity. Figure 14 shows a combined plot of, first, the wavenumber at which the turbulence-to-ambiguity ratio is unity and, second, the wavenumber of half-power attenuation to which the spectrum may be corrected by subtracting the ambiguity ($\sin\frac{1}{2}\theta$ has been chosen as 0·145). By choosing values of $\tilde{k}_*$ greater than $\tilde{k}_{*\mathrm{opt}}$ the half-power attenuation may be moved to as high a wavenumber as we please; however, the Doppler ambiguity will be sharply increased as will the error involved in obtaining the corrected spectral values.

To summarize the above comments into a practical plan for research: in all but the most unusual circumstances, the size of the scattering volume should be determined by (6.2.2) for minimum ambiguity; the spectral values obtained should then be corrected by subtracting the Doppler ambiguity; and finally, the corrected values should be multiplied by the inverse transfer function $F_{11}^{1}(k)/F_0(k_1)$ to determine the true spectrum.

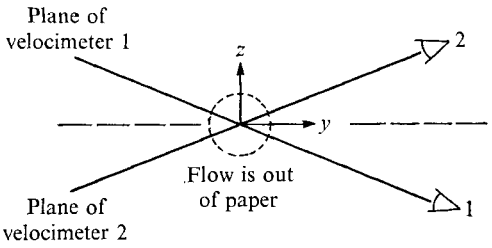

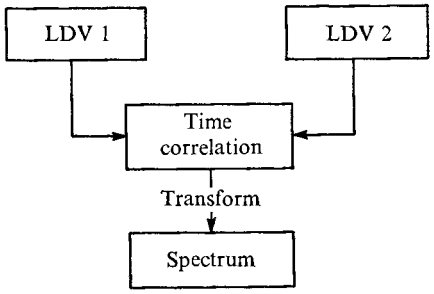

FIGURE 15. Technique for eliminating ambiguity by cross-correlation.

6.3. *Possible alternatives for spectral measurement*

It has been suggested by some investigators that the Doppler ambiguity might be eliminated by using a frequency-tracking device. A frequency tracker basically averages the product of the signal and the frequency of a local oscillator, adjusting the local oscillator frequency to minimize the mean product. It is thus seen to be equivalent to a filter, operating on the input slewing rate, the filter characteristic being determined by the loop gain and the averaging characteristic. If the slewing rate $\dot{\phi}$ of the phase fluctuations due to the Doppler ambiguity were significantly different from the slewing rate ω_0 of the turbulence, the averaging time of the frequency tracker might be adjusted to average out the ambiguity fluctuations. Unfortunately, this attractive possibility does not correspond to reality; an examination of the spectra reveals that the slewing rates of the ambiguity and turbulence are quite similar and thus indistinguishable on the basis of second-order statistics. Clearly the frequency tracker can remove the Doppler ambiguity only by also removing some of the turbulence.

It was pointed out in § 5.7 that two-point correlations may be performed by using two velocimeters since the Doppler ambiguity is uncorrelated if the scattering volumes do not overlap. If sufficient accuracy in determining the spectrum is not obtainable using the subtraction procedure suggested above, we may use two velocimeters whose scattering volumes are very close to each other – say within the turbulence microscale – although not overlapping; figure 15 shows a possible configuration. After performing time correlations between the two outputs, we may obtain the spectrum by Fourier transforming the corre-

Application	Radiation	λ	Velocity (m/s)	ν_D	R	$\tilde{k}_0$
Grid turbulence in water	Light	0·6 μm	1	500 kHz†	2	0·5
Grid turbulence in air	Light	0·6 μm	1	500 kHz†	0·3	0·8
Wakes in air	Light	0·6 μm	300	150 MHz†	40	0·1
Clear-air turbulence	Radar	1 cm	1‡	100 Hz§	600	0·01
Oceanic turbulence	Sonar	0·01 cm	1‡	20 kHz§	50	0·1

† $\sin \frac{1}{2}\theta \sim 0{\cdot}1$, ‡ No mean velocity; $u' \sim 1$ m/s. § Backscattering; $\sin \frac{1}{2}\theta/2 \sim 1$.

TABLE 1

lation. Since the Doppler ambiguities of the two velocimeters are uncorrelated and since the velocimeters are essentially sampling the same velocity fluctuation, the measured correlation is simply the correlation of the turbulence alone as is the resulting spectrum. Clearly, the spectrum can only be resolved to scales corresponding to the separation between the scattering volumes. This method of measuring spectra suffers from several obvious disadvantages: it requires two velocimeters instead of one, it requires very careful alignment to avoid overlapping and crosstalk, and considerable added effort is necessary to correlate and transform the outputs.

6.4. *Conclusions*

The influence of the Doppler ambiguity, together with the problems of resolution, have been shown to provide major limitations on the use of the laser-Doppler velocimeter in the measurement of turbulence.

It should be noted that these limitations apply to all Doppler velocimeters regardless of the incident radiation. Table 1 shows an estimate of the dimensionless wavenumber at which the turbulence-to-ambiguity ratio is unity for a number of different applications. These estimates show that the possibility of measuring dissipation spectra in high-speed or in geophysical flows using Doppler velocimeters is quite remote.

Part 2. Experimental verification

7. The apparatus

7.1. *The optical system*

The optical system used in these experiments is of the type proposed by Goldstein and is shown in figure 16. The system was chosen for its simplicity and for the ease with which it could be aligned.

The source of radiation was a nominal 50 mW neon–helium laser (Spectra-Physics Model 125); the actual output was closer to 90 mW. The beam was vertically polarized and of Gaussian cross-section. The distance between the $1/e^2$ points of intensity was about 2 mm and the divergence angle was less than 0·7 mrad.

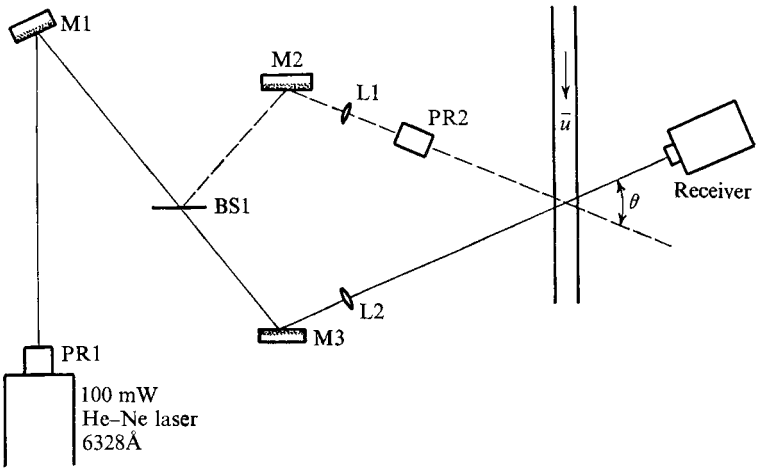

FIGURE 16. Optical arrangement. L1, L2, lenses; PR1, PR2, polarization rotators; M1, M2, M3, front surface mirrors; BS1, polarizing beam splitter. $\omega_0 = 2\pi(2u/\lambda)\sin\frac{1}{2}\theta$.

The beam was split into the reference and scattered beams by means of a polarized beam splitter which passed only horizontally polarized light. By rotating the plane of polarization of the incoming light with a polarization rotator (Spectra-Physics Model 310), the relative intensity of the two beams could be adjusted for the optimum signal strength. A second polarization rotator served to return the horizontally polarized beam to being vertically polarized since the scattering intensity is maximized when the polarization of the light is perpendicular to the plane of scattering (which in our case was horizontal).

The two beams were focused to the desired region in the flow with spherical lenses obtained from Ealing Optical. Since the f-number based on beam diameter in our experiments ranged from 50 to 1000, aberrations were negligible and the lenses were diffraction-limited to a high approximation. Precise alignment was afforded by micrometer mirror mounts (Oriel Model 145) in the reference and scattered beams.

The entire optical system rested on a 700 lb concrete table supported by four viscoelastic sandwich pads. This arrangement served to minimize vibrations to the point where no realignment of the optics was necessary over run periods up to 3 h.

The test section was circular in cross-section and constructed of Plexiglas tubing. To minimize the lens effect of the test section, an optically flat box was placed around the test section and filled with water so as to provide an approximately constant index of refraction. No additional optical filters or apertures were present between the flow and the photodiode.

7.2. *The scattering agent*

Because of the large quantity of scattering particles necessary for a 1000-gallon facility, an inexpensive supply was necessary. Homogenized milk in concentrations of about 1:2000 was found to provide an excellent signal-to-noise ratio.

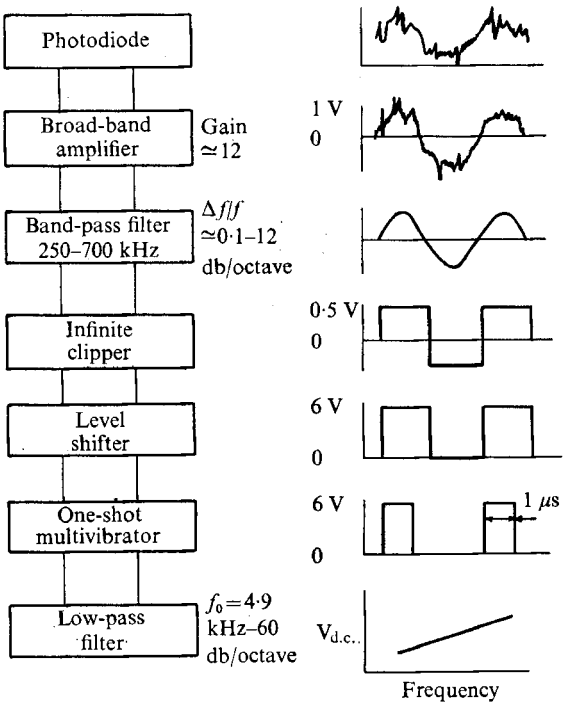

FIGURE 17. Signal processor.

From Clayton, the average fat particle size is approximately 0·3 μm with about 10^{14} particles per litre of milk; hence, the particle concentration was approximately 5×10^7 particles per c.c.

7.3. *The optical receiver*

The heart of the receiver package was an EG & G Model SDG-040A photodiode (surface area $\sim$ 0·1 cm^2). This was chosen because of its high quantum efficiency ($\sim$ 50 %) and low cost ($\sim$ \$15·00). The photodiode was biased at 90 V with standard mercury cells. The noise was primarily due to the input noise from the first amplifier stage; this represented a distinct improvement over previous attempts to use a photomultiplier tube where, because of the much lower quantum efficiency, the noise was predominantly photon shot noise from the reference beam. With use of the latest avalanche and combination diodes, the noise in our set-up could probably have been reduced to the shot noise limit, but this was not deemed necessary.

The photodiode was followed by a single broad-band amplifier having a gain of 12, a tunable band-pass filter (250–700 kHz) with a bandwidth of about 10 %, and an infinite clipper (gain $\sim$ 140 db) which effectively removed all the amplitude information. Signal-to-noise ratios measured after the filter by blocking the scattering beam typically ranged from 10 to 50.

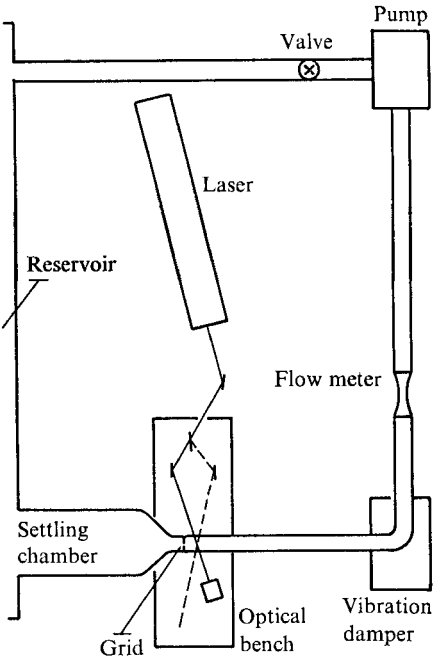

FIGURE 18. Flow facility.

7.4. *Frequency-to-voltage convertor*

The frequency-to-voltage convertor, together with the optical receiver package, is shown in figure 17. The frequency-to-voltage convertor was constructed from standard Honeywell 5 mc microcircuits (μ-PACS) along with a -60 db/octave Butterworth low-pass filter (Wyngaard & Lumley 1967). The response was linear to inputs between 8 kHz and 1 MHz to within 3 %.

7.5. *The flow facility*

The facility used in these experiments is shown diagrammatically in figure 18. It is essentially a closed-circuit water tunnel with a 1·7 in. I.D. circular test section. The flow passes from a 1000-gallon reservoir into a long settling chamber 12 in. in diameter by 30 in. From the settling chamber the flow enters the test section through a 36 : 1 contraction. The flow is pulled through the test section by a pump which permits flow rates up to 10 m/s; the flow rate is controlled by varying the pump speed or by adjusting the valve in the return system. The mean flow rate shows negligible drift over periods up to an hour and the root-mean-square velocity fluctuation with no grid is less than 0·2 % of the mean flow rate.

For the turbulence experiments a grid was inserted at the end of the contraction. The grid was of biplane design and was constructed of no. 19 hypodermic tubing. The bar spacing was 0·1 in.; this corresponded to a solidity of 0·32, which was close to that used by other investigators of homogeneous turbulent flows (cf. Comte-Bellot & Corrsin 1966).

Mean flow velocities were measured with a Potter flow meter (Model 1-5550)

which was installed after the test section. The meter produced a signal whose frequency was proportional to the mean flow rate. The frequency of the flow meter output was monitored with a counter and flow rates were read from the calibration curve, which was linear over the range of velocities used.

7.6. *The measurement of spectra and correlations*

Spectra were measured by feeding the amplitude-modulated signal from the detector of the laser-Doppler velocimeter into a Hewlett–Packard Model (302A) Wave Analyser (equivalent noise bandwidth 6 c/s). The internal 100 kHz carrier from the wave analyser was squared by a Ballantine true r.m.s. voltmeter (Model 320A) and integrated for 60 s by an analog integrator yielding a d.c. output proportional to the spectral height. The system was calibrated independently with a low-passed white noise signal.

Analysis of the data reveals a consistent decrepancy between experiment and theory which can be traced only to an incorrect calibration. Unfortunately, this apparent error was discovered too late to be rectified and the data are presented as originally taken.

Correlations were performed with a PAR correlator having a time constant of 10 s.

8. The measurements

8.1. *Background*

Spectral measurements were taken in both laminar and turbulent flow in water in an attempt to identify the separate effects of finite particle transit times and the turbulent fluctuations across the beam. In all cases the effect of the noise was less than 1 %.

The flow velocities varied from 70 to 100 cm/s and the Doppler beat frequencies from 250 to 650 kHz. This corresponded to values of R from about 1 to 3.

8.2. *Laminar flow*

Figure 19 shows measured spectra in laminar flow. The measurements were non-dimensionalized by the Doppler bandwidth calculated from the flow velocity and lens focal length. The dependence of the height of the ambiguity spectrum on the transit time $\Delta\omega = (1/k_*\overline{U})$ is clearly shown in figure 20, in which the spectral height is plotted as a function of k_*. In both cases, the data are about 65 % high. Analysis of the turbulent data presented below reveals that this error must be in calibration.†

8.3. *Turbulent flow*

The measurements in turbulent flow were taken 45 mesh lengths behind the grid, where the turbulence is approximately isotropic. Spectra were non-dimensionalized by ν and the rate of dissipation ϵ determined from the measured

† It has here been assumed that Rice's prediction of the spectral height is correct and his theory applicable. This assumption is supported by the observations of other investigators (Berman & Dunning 1973).

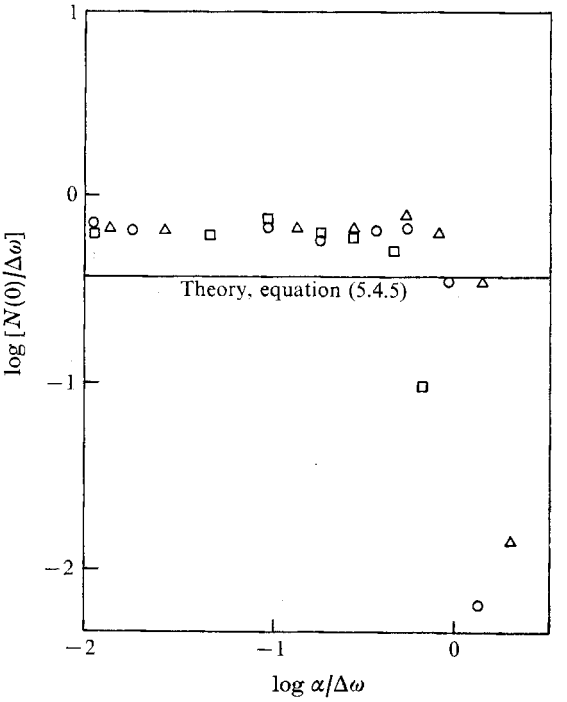

FIGURE 19. Measured ambiguity spectra in laminar flow. $\Delta\omega = k_* \bar{u}$, $\bar{u} = 80$ cm/s. △, $k_* = 282$ cm^{-1}; ○, $k_* = 352$ cm^{-1}; □, $k_* = 470$ cm^{-1}.

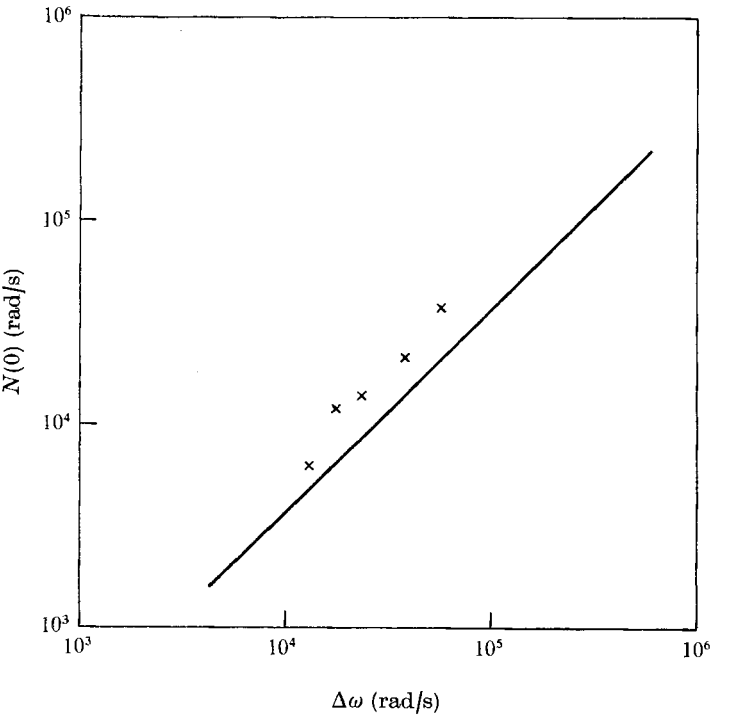

FIGURE 20. Dependence of spectral height $N(0)$ on $\Delta\omega = \bar{u}k_*$ (k_* calculated from lens focal length). ——, $N(0) = 0{\cdot}368\Delta\omega$. Uniform laminar flow; $\bar{u} = 80$ cm/s.

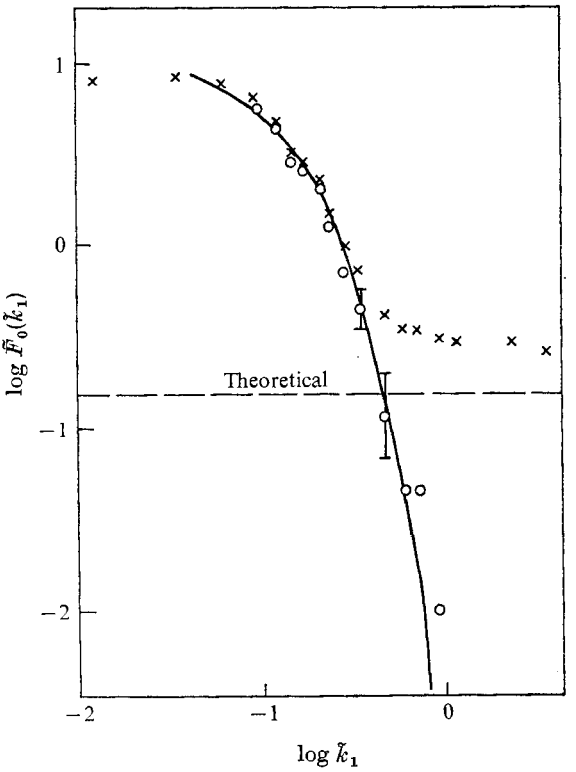

FIGURE 21. Measured (crosses) and corrected (circles) spectra in turbulent flow shown with spectrum measured with hot-film anemometer. $R_M = 2 \times 10^3$, $x/M = 45$, $\tilde{k}_* = 3{\cdot}9$, $\sin \frac{1}{2}\theta = 0{\cdot}145$.

decrease in turbulent intensity with distance from the grid. The intensity measurements were taken with a hot-film anemometer because of the high ambiguity-to-turbulence ratio in such a low intensity flow.

A typical turbulence spectrum is shown in figure 21. The measured spectral values are seen to approach a constant value and then to drop slowly; the slow drop-off seems to begin at about the wavenumber corresponding to $\alpha \sim \Delta\omega$ as predicted. The constant value was subtracted from the measured spectral values; the result is seen to be within experimental error of that measured with a constant temperature hot-wire anemometer and a conical hot-film probe.

Corrected spectral measurements for six different values of $\tilde{k}_*$ are shown in figure 22. The smallest value of $\tilde{k}_*$ used (0·55) corresponds to a value of $\tilde{m}_* = 0{\cdot}08$. Clearly, as expected from the analysis of §3.1, this set of measurements shows considerable attenuation ($\sim 50\,\%$) at all wavenumbers. Because of the low Reynolds number (deviation from Pao's spectrum at low wavenumbers) and the large error at high wavenumbers, it was not possible to perform an accurate check on the transfer function given in § 3.1.

Figure 23 shows the measured ambiguity spectral height (determined from the asymptotic values of the turbulent spectra) as a function of $\tilde{k}_*/\tilde{k}_{*\mathrm{opt}}$, where $\tilde{k}_{*\mathrm{opt}}$ is computed from (5.10.5). The asymptotic theory is *not* applicable here because

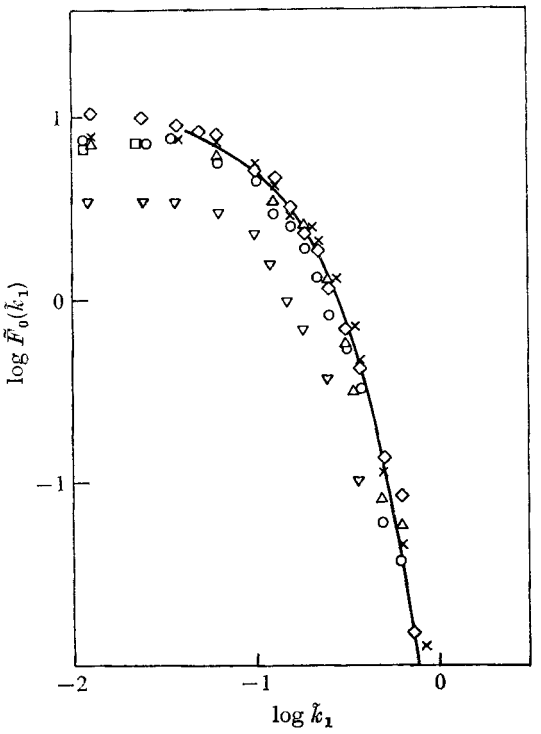

FIGURE 22. Corrected spectra shown with spectrum measured with hot-film anemometer. $R_M = uM/\nu = 2\times10^3$, $\sin\frac{1}{2}\theta = 0{\cdot}145$.

	▽	○	◇	×	□	△
$\tilde{k}_*$	0·55	1·1	2·2	3·9	5·5	7·4

of the relatively small values of $\tilde{m}_*$. Likewise, the turbulent bandwidth computed from Pao's spectrum is too high since it is clear from the measured spectra that the velocity fluctuations at low wavenumbers are overestimated. The transverse spectrum $F^2_{11}(k_2)$ was computed from the longitudinal spectrum $F^1_{11}(k_1)$ obtained from the laser-Doppler velocimeter measurements and this was used in (3.2.10) to compute the turbulent bandwidth $\Delta\omega_T$. As before, the measured values are above the theoretical curve. If this error were other than from calibration, the minimum would occur in the wrong place.

Figure 24 shows time autocorrelations at two distances from the grid (no attempt was made to calibrate the vertical axis). The effect of the ambiguity is dramatically illustrated in spite of the 5 kHz low-pass filter in the detector.

8.4. *Conclusions*

The measurements taken in both laminar and turbulent flow show the trends predicted by theory. Since there are no adjustable constants in either theory or experiment in the prediction of the results of figure 23, these results must be regarded as conclusive and the theory substantially correct.

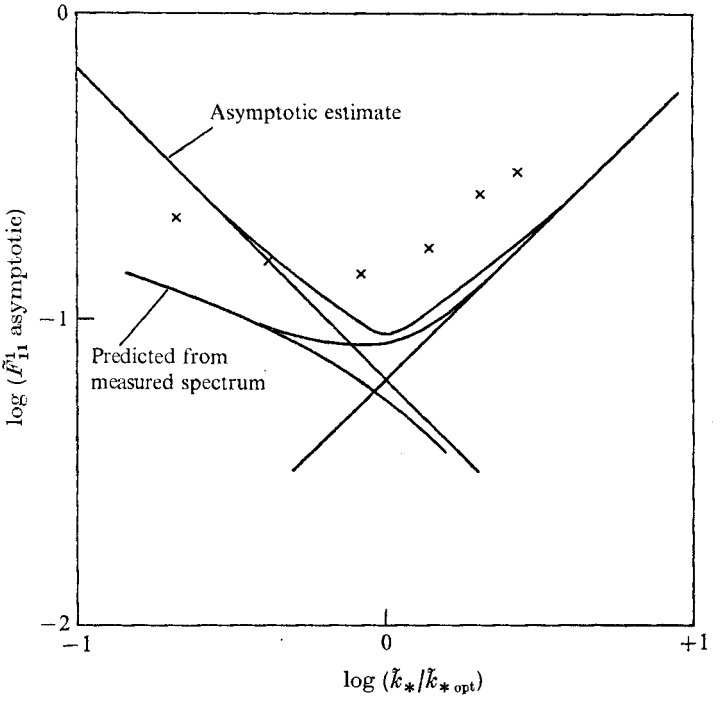

FIGURE 23. Typical turbulence autocorrelations illustrating the effect of the low-passed Doppler ambiguity.

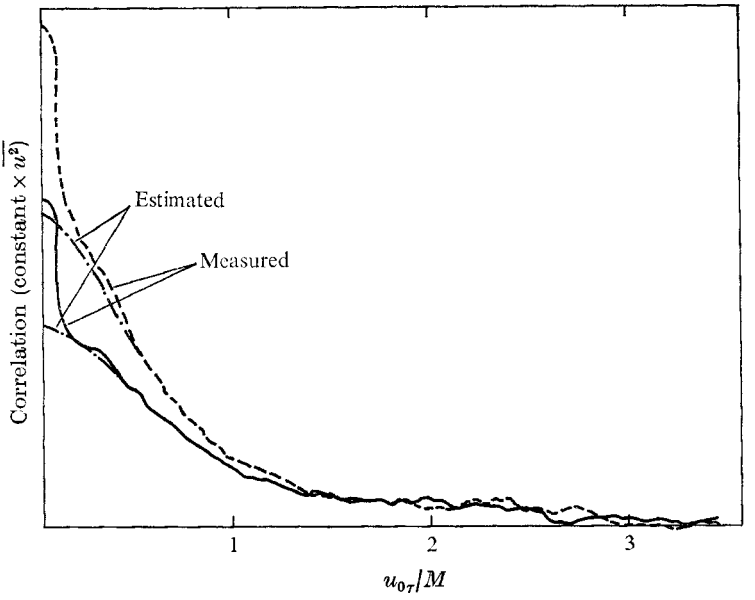

FIGURE 24. Turbulence autocorrelations at two distances from the grid. $R_M = u_0 M/\nu = 2500$. – – –, $x/M = 40$; ——, $x/M = 70$.

The authors would like to thank Professor H. Tennekes and Professor N. Berman for many stimulating discussions of this material. We are also grateful to R. Pierce and E. Jordan, who assisted in the design and construction of the electronics, to T. Gatski and R. Carlson, who assisted with the measurements, to K. Jones, who assisted with the computer programming, and to P. Stover for typing the manuscript.

Earlier versions of portions of this material have appeared in Lumley *et al.* (1969) and George & Lumley (1970, 1971), as well as in the first author's doctoral dissertation presented to the Department of Mechanics of the Johns Hopkins University.

This research was supported in part by the Office of Naval Research under Contracts Nonr656(33) and N00014-67-A-0385-0013 with the Pennsylvania State University and in part by the Applied Research Laboratory of the Pennsylvania State University under contract with the Naval Ordnance Systems Command.

Appendix

$g(\mathbf{x})$ has been defined as a random weighting function which accounts for the presence or absence of the scattering particles, as well as their size. For convenience, we define

$$g(\mathbf{x}) = g_1(\mathbf{x})\, A(\mathbf{x}), \tag{A 1}$$

where $g_1(\mathbf{x})$ accounts for the presence or absence of the scattering particles and $A(\mathbf{x})$ accounts separately for the particle size – in this context its scattering coefficient C_p. For dilute solutions, $g_1(\mathbf{x})$ and $A(\mathbf{x})$ are statistically independent.

If N_i is the instantaneous number of particles in the scattering volume V, we have

$$N_i = \int_V g_1(\mathbf{x})\, d\mathbf{x} \tag{A 2}$$

and

$$\overline{N_i} \equiv N_V = \int_V \overline{g_1(\mathbf{x})}\, d\mathbf{x} = \overline{g_1(\mathbf{x})} \cdot V \tag{A 3}$$

since $g_1(\mathbf{x})$ is homogeneous. Therefore

$$\overline{g_1(\mathbf{x})} = N_V/V = \mu, \tag{A 4}$$

where μ is the expected number of particles per unit volume.

The scattering particles are usually distributed as Poisson random variables; hence, if $P(N_i)$ is the probability of having N_i particles in the volume, we have (Rice 1954)

$$\overline{N_i^2} = \sum_{N_i=0}^{\infty} N_i P(N_i) = \mu V(1+\mu V). \tag{A 5}$$

We also have

$$\overline{N_i^2} = \iint_V \overline{g_1(\mathbf{x})\, g_1(\mathbf{x}')}\, d\mathbf{x}\, d\mathbf{x}'. \tag{A 6}$$

Using generalized functions (Lumley 1970)

$$\iint_V \phi(\mathbf{x}, \mathbf{x}')\, d\mathbf{x}\, d\mathbf{x}' = \mu^2 V^2 \tag{A 7}$$

has the solution $\phi = \mu^2$ and

$$\iint_V \phi(\mathbf{x}, \mathbf{x}')\, d\mathbf{x}\, d\mathbf{x}' = \mu V \tag{A 8}$$

has the solution $\phi = \mu\delta(\mathbf{x} - \mathbf{x}')$. Hence,

$$\overline{g_1(\mathbf{x})\, g_1(\mathbf{x}')} = \mu^2 + \mu\delta(\mathbf{x} - \mathbf{x}'). \tag{A 9}$$

For a monodisperse particle distribution normalized to unit size, $g(\mathbf{x}) = g_1(\mathbf{x})$. Since $g_1(\mathbf{x})$ and $A(\mathbf{x})$ are statistically independent, the extension of the above results to arbitrary particle distributions is straightforward.

REFERENCES

Batchelor, G. K. 1960 *The Theory of Homogeneous Turbulence.* Cambridge University Press.

Berman, N. S. & Dunning, J. W. 1973 *J. Fluid Mech.* to be published.

Clark, W. H. 1970 Measurement of two-point velocity correlations in a pipe flow using laser velocimeters. Ph.D. thesis, Department of Aerospace Engineering, University of Virginia, Charlottesville.

Clayton, W. 1954 *Emulsions and Their Technical Treatment.* London: Churchill.

Comte-Bellot, G. & Corrsin, S. 1966 The use of a contraction to improve the isotropy of grid-generated turbulence. *J. Fluid Mech.* **25**, 657–682.

Davis, D. T. 1968 Analysis of a laser-Doppler velocimeter. *I.S.A. Trans.* **7**, 43–51.

Edwards, R. V., Angus, J. C., French, M. J. & Dunning, J. W. 1971 Spectral analysis of the signal from the laser-Doppler velocimeter: time-independent systems. *J. Appl. Phys.* **42**, 837–850.

Foreman, J. W., Lewis, R. D. & Thornton, J. R. 1966 Laser-Doppler velocimeter for measurement of localized fluid velocities in liquids. *Proc. I.E.E.E.* 424.

George, W. K. 1971 An analysis of the laser-Doppler velocimeter and its application to the measurement of turbulence. Ph.D. thesis, Department of Mechanics, The Johns Hopkins University.

George, W. K. & Lumley, J. L. 1970 Limitations on the measurement of turbulence using a laser-Doppler velocimeter. *Proc. Electro-Optical Conf., New York*, p. 926.

George, W. K. & Lumley, J. L. 1971 The measurement of turbulence with a laser-Doppler velocimeter. *A.S.C.E. Conf. Water Resources, Phoenix*, no. 1345.

Goldstein, R. J. & Kreid, D. K. 1967 Turbulent flow measurements utilizing the Doppler shift of scattered laser radiation. *Phys. Fluids*, **10**, 1349.

Goodman, J. W. 1968 *Introduction to Fourier Optics.* McGraw-Hill.

Greated, C. A. 1969 Effect of polymer additives on grid turbulence. *Nature*, **224**, 1196–1197.

Huffaker, R. M., Fuller, C. E. & Lawrence, T. R. 1969 Application of laser-Doppler velocity intrumentation to the measurement of jet turbulence. *Int. Automotive Engng Congress, Detroit, Michigan.*

Lading, L. 1970 Differential Doppler heterodyning technique. *Appl. Optics*, **10**, 1943–1949.

Lawson, J. L. & Uhlenbeck, G. E. 1950 *Threshold Signals.* McGraw-Hill.

Lhermitte, R. M. 1968 Turbulent air motion as observed by Doppler radar. *Proc. 13th RADAR Meteor. Conf., McGill University, Montreal.*

Little, C. G. 1969 Acoustic methods for the remote probing of the lower atmosphere *Proc. I.E.E.E.* **57**, 571–578.

LUMLEY, J. L. 1961 The mathematical nature of the problem of relating Lagrangian and Eulerian statistical functions in turbulence. *Mécanique de la Turbulence*. Paris: C.N.R.S.

LUMLEY, J. L. 1970 *Stochastic Tools in Turbulence*. Academic.

LUMLEY, J. L., GEORGE, W. K. & KOBASHI, Y. 1969 The influence of Doppler ambiguity and noise on the measurement of turbulent spectra using a laser-Doppler velocimeter. *Proc. Symp. on Measurement of Turbulence in Liquids, University of Missouri at Rolla*, p. 3.

LUMLEY, J. L. & PANOFSKY, H. A. 1964 *The Structure of Atmospheric Turbulence*. Interscience.

MAYO, W. T. 1969 Laser-Doppler flowmeter – a spectral analysis. Ph.D. thesis, Department of Electrical Engineering, Georgia Institute of Technology.

MAYO, W. T. 1970 Spatial filtering properties of the reference beam in an optical heterodyne receiver. *Appl. Optics*, **9**, 1159–1162.

MIDDLETON, D. 1950 Spectrum of frequency-modulated waves. *Quart. Appl. Math.* **8**, 59–81.

PAO, Y. H. 1965 Structure of turbulent velocity and scalar fields at large wavenumbers. *Phys. Fluids*, **8**, 1063.

PIKE, E. R., JACKSON, D. F., BOURKE, P. J. & PAGE, D. I. 1967 Measurement of turbulent velocities from the Doppler shift in scattered laser light. *Presentation at Div. Fluid Dyn., Am. Phys. Soc., Lehigh.*

RICE, S. O. 1948 Statistical properties of a sine wave plus random noise. *Bell Syst. Tech. J.* **27**, 109–157.

RICE, S. O. 1954 Mathematical analysis of random noise. *Selected Papers on Noise & Stochastic Processes* (ed. N. Wax), p. 133. Dover.

ROLFE, E., SILKE, J. K., BOOTH, S., MEISTER, K. & YOUNG, R. M. 1968 Laser-Doppler velocity instrument. *N.A.S.A. Current Rep.* no. 1199.

SERRIN, J. 1959 Mathematical principles of classical fluid mechanics. In *Handbuch der Physik*, vol. 8 (ed. S. Flugge), p. 1. Springer.

VAN DE HULST, H. C. 1957 *Light Scattering by Small Particles*. Wiley.

WELCH, N. E. & TOMME, W. J. 1967 Analysis of turbulence from data obtained with a laser-Doppler velocimeter. *A.I.A.A. Paper*, no. 67–179.

WISEMAN, W. J. 1969 On the structure of high frequency turbulence in a tidal estuary. *Chesapeake Bay Inst., The Johns Hopkins University, Tech. Rep.* no. 59.

WYNGAARD, J. C. 1968 Measurement of small-scale turbulence structure with hot wires. *J. Sci. Instrum.* **1**, 1105.

WYNGAARD, J. C. & LUMLEY, J. L. 1967 A sharp cutoff spectral differentiator. *J. Sci. Instrum.* **44**, 363–365.

YEH, H. & CUMMINS, H. Z. 1964 Localized fluid flow measurements with He–Ne laser spectrometer. *Appl. Phys. Lett.* **4**, 176.